β-decay studies of neutron-rich K isotopes

F. Perrot,[1] F. Maréchal,[1] C. Jollet,[1] Ph. Dessagne,[1] J.-C. Angélique,[2] G. Ban,[2] P. Baumann,[1] F. Benrachi,[3] U. Bergmann,[4] C. Borcea,[5] A. Buţă,[5] J. Cederkall,[4] S. Courtin,[1] J.-M. Daugas,[6] L. M. Fraile,[4] S. Grévy,[2] A. Jokinen,[7] F. R. Lecolley,[2] E. Liénard,[2] G. Le Scornet,[4] V. Méot,[6] Ch. Miehé,[1] F. Negoiţă,[5] N. A. Orr,[2] S. Pietri,[2] E. Poirier,[1] M. Ramdhane,[3] O. Roig,[6] I. Stefan,[5] and W. Wang[7]

[1]*Institut de Recherches Subatomiques, IN2P3-CNRS et Université Louis Pasteur, F-67037 Strasbourg Cedex 2, France*
[2]*Laboratoire de Physique Corpusculaire, ENSICAEN et Université de Caen, IN2P3-CNRS, F-14050 Caen Cedex, France*
[3]*Department of Physics, Mentouri Constantine University, 25000 Constantine, Algeria*
[4]*ISOLDE, Division EP, CERN, CH-1211 Geneva, Switzerland*
[5]*Institute of Atomic Physics, IFIN-HH, Bucharest, Romania*
[6]*CEA/DIF/DPTA/SPN, BP 12, F-91680 Bruyères-le-Châtel, France*
[7]*Department of Physics, University of Jyväskylä, FIN-40351 Jyväskylä, Finland*

(Received 25 April 2005; revised manuscript received 12 January 2006; published 21 July 2006)

The β decay of the neutron-rich nuclei $^{51-53}$K has been used to populate bound and unbound states in $^{50-53}$Ca. Measurements of γ rays as well as β-delayed neutrons enabled detailed decay schemes to be established and levels identified in $^{50-53}$Ca. A delayed one-neutron emission probability P_{1n} of $63 \pm 8\%$ was determined for the decay of ^{51}K. A total of seven new γ transitions were observed following the decay of ^{51}K, and 25 neutron branches were found that enrich the level scheme of ^{51}Ca. Delayed neutron emission probabilities of $P_{1n} = 74.4 \pm 9.3\%$ and $P_{2n} = 2.3 \pm 0.3\%$ were determined for the decay of ^{52}K, and 12 new γ transitions were observed in ^{50,51,52}Ca. Three new γ transitions were observed in ^{52,53}Ca following the β decay of ^{53}K. New limits on the P_{1n} and P_{2n} values were determined for the β decay of ^{53}K, and a decay scheme was established for ^{53}Ca for the first time. The data obtained here should help clarify the structure of neutron-rich fp-shell nuclei around the $N = 32$–34 subshell closures.

DOI: 10.1103/PhysRevC.74.014313 PACS number(s): 23.40.−s, 23.20.Lv, 27.40.+z

I. INTRODUCTION

Following the inclusion of a spin-orbit force in the nuclear potential [1,2], the shell model has become a powerful predictive tool in nuclear structure, reproducing, for example, the known magic numbers near stability. However, the valley of β stability represents only a very limited region of the nuclear landscape, and making extrapolations to new regions is not trivial. In this respect, the study of very neutron-rich isotopes provides a fertile testing ground for our understanding of nuclear shell structure far from stability.

Recently, work has shown that the attractive $\pi j_> - \nu j_<$ monopole term in the nucleon-nucleon interaction plays an important role in defining the magic numbers in exotic nuclei [3]. The effect of this proton-neutron interaction on the location of single-particle states has been invoked to account for the appearance of an $N = 32$ subshell closure for neutron-rich nuclides in the fp shell [4]. Indeed, the relatively high energy of the 2_1^+ state experimentally observed in ^{56}Cr [5,6], ^{54}Ti [7], and ^{52}Ca [8] can be explained by the reduced monopole interaction shifting the $\nu f_{5/2}$ orbital to higher energies when protons are removed from the $\pi f_{7/2}$ orbital. A similar effect is seen in the $N = 29$ isotones for which a 3 MeV energy shift of the $\nu f_{5/2}$ state is observed when protons are added to the $\pi f_{7/2}$ orbital going from ^{49}Ca to ^{57}Ni [9,10]. Calculations using the recent effective interaction GXPF1 show that $N = 34$ could be a new magic number for neutron-rich isotopes with $Z \leqslant 22$ [3]. However, this has not yet been experimentally proven for $^{56}_{22}$Ti, and the question remains open for the calcium isotopes [11].

The neutron-rich calcium isotopes are indeed interesting to study, in particular as they allow the ν-ν matrix elements of the effective interaction to be determined in the $A = 50$ mass region. Owing to the $Z = 20$ shell closure, the lowest energy states in even Ca isotopes are of positive parity. These natural parity states are populated either by forbidden transitions (β decay) or indirectly (γ cascade) and their properties (E_x, decay modes) are governed by the neutron-neutron monopole interaction in the fp shell. They are thus indicative of the neutron subshell sequence. New experimental data should, therefore, allow us to test the shell model in the $A \sim 50$ mass region, in which modifications of the shell structure are expected and for which experimental data are still lacking.

The present work investigates the β decay of $^{51-53}$K using γ and delayed neutron spectroscopy in order to complete our knowledge of the low-lying level structure of the neutron-rich calcium isotopes. Here, we focus on the experimental results for decays to states in $^{50-53}$Ca. The paper is organized as follows. The experimental procedures are described in Sec. II. Section III presents the data analysis. Results for the decay of each isotope are presented and discussed separately in detail in Secs. IV–VI. Finally, conclusions are drawn in Sec. VII.

II. EXPERIMENT

The experiment was carried out at the ISOLDE online isotope mass separator facility at CERN [12]. The radioactive

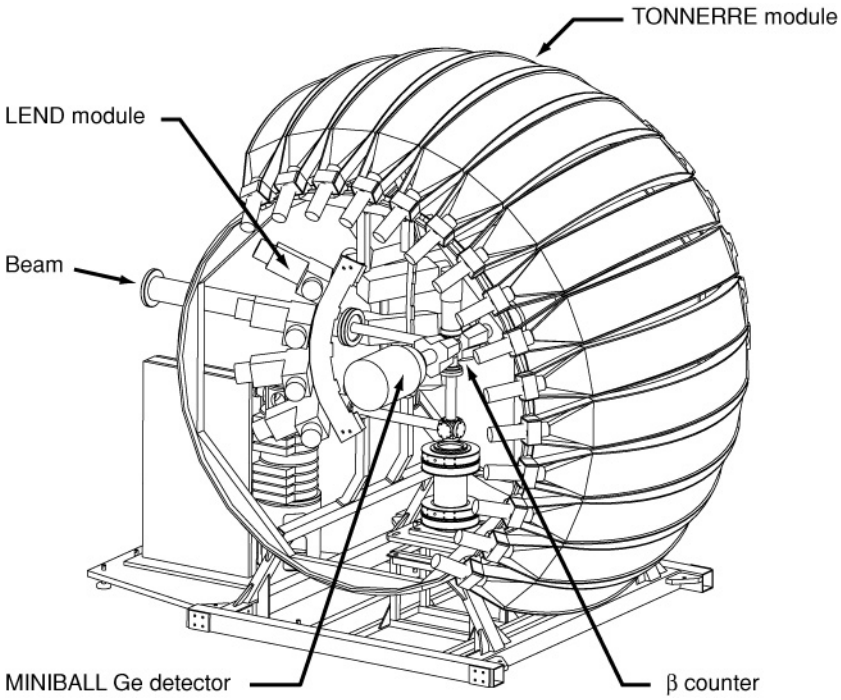

FIG. 1. Schematic view of the experimental setup. Radioactive ions were implanted on the tape located at the center of the β counter. γ rays were detected using two MINIBALL Ge detectors, while the delayed neutrons were registered by the TONNERRE array at forward angles and by the LEND module at backward angles.

K ion beams were produced by spallation of a thick (53 g/cm^2) UC_x target induced by an intense (5 μA) 1.4 GeV proton beam delivered by the CERN proton-synchroton booster (PSB). A hot transfer line connected the target and the tungsten surface ion source, from which the ions were extracted in the 1^+ charge state and electrostatically accelerated to 60 keV. The spallation products were analyzed using the high resolution separator (HRS) and collected on a 55 μm thick aluminized Mylar tape. The average production yields for ^{51}K, ^{52}K, and ^{53}K were 2.3×10^3, 50, and 2 atoms/μC, respectively. The beam optics were set using a beam of ^{39}K, and a transmission of 90% was achieved over the 25 m flight path between the HRS and the experimental setup.

Figure 1 shows a schematic view of the experimental setup. The β particles were detected in a 2 mm thick cylindrical plastic scintillator surrounding the collection point in a near 4π geometry with a total detection efficiency of 71(5)%. The β-counter signal was the sole acquisition trigger (i.e., master trigger) and was used to time-stamp the events and to start the neutron time-of-flight measurements. Hence, the β-detection efficiency is only relevant for the determination of the K isotope production yields. The γ rays were measured using two large Ge clusters from the MINIBALL array [13] placed on either side of the beam and positioned 29 mm from the implantation point. The energy resolution for each Ge crystal was measured to be ~3 keV (full width at half maximum) for the 1.33 MeV γ-ray transition in ^{60}Co. Absolute γ-detection efficiencies were determined using ^{152}Eu and ^{232}Th sources of known activities. The total photopeak efficiency was 5.1% at 1.33 MeV.

The β-delayed neutrons were detected using two types of detectors, and their energies were measured using the time-of-flight technique. For low-energy neutrons, a group of six low-energy neutron detectors (LENDs), each consisting of a 1 cm thick BC400 plastic scintillor (10 cm diameter) readout by two photomultiplier tubes (PMTs) operated in coincidence, were employed with a 66 cm flight path [14]. With the PMT threshold adjusted to be just below the one photoelectron level, the neutron energy threshold was approximately 60 keV. For the higher energy neutrons, 11 curved (120 cm flight path) BC400 scintillating plastic bars from the TONNERRE array were employed [15]. Each individual bar ($160 \times 20 \times 4$ cm^3 volume) was readout by a photomultiplier tube at each end. The neutron detection threshold for these modules was about 150 keV. The absolute neutron detection efficiency for both groups of detectors was derived from the observed intensities of the well-known β-delayed neutron decay of ^{49}K [16,17]. Total efficiencies (including the solid angle) for the LEND and TONNERRE modules are 2.0% and 7.7% at 1 MeV, respectively. Energy resolutions of 6% and 11% were measured at 440 keV for the two neutron detection systems, respectively.

The CERN PSB delivers a pulsed proton beam over a "supercyle" of 19.2 s. Within this supercycle, a total of 16 proton pulses, each 1.2 s apart, are shared among the different users. During our experiment, only 6–10 of the 16 proton pulses were delivered to the ISOLDE production target. Each measurement cycle (Fig. 2) had a duration T_m, greater than five times the half-life of the implanted K isotope, and was delayed by a time T_d with respect to the proton pulse to avoid contamination of our measurements by the prompt neutron flash from the target. The ions were collected on the Mylar tape for a time T_c at the beginning of each cycle (beam gate opened). Table I summarizes these different parameters as well as the total counting time T_{acq} devoted to the study of each K isotope decay. During each measurement cycle, β-γ as well as β-n, β-γ-γ, and β-n-γ coincidences were registered. At the beginning of each cycle, a universal time clock was started and the time of each event was recorded. The tape was moved at the end of each supercycle in order to limit the buildup of daughter activity.

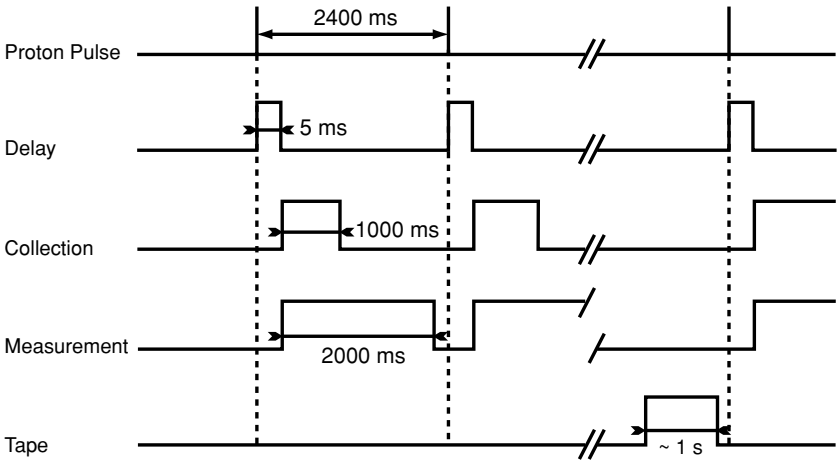

FIG. 2. Time line of the acquisition cycles. Each measurement phase T_m was delayed by a time T_d with respect to the proton pulse. The ions were collected on the tape for a time T_c at the beginning of each cycle, and the tape was moved at the end of each supercycle.

III. DATA ANALYSIS

A. β activity

To obtain absolute branching ratios to levels in the daughter nuclei and delayed neutron emission probabilities, the total number of decays N_β had to be precisely determined. This was obtained from a careful analysis of the corresponding activity spectrum (see, for example, Fig. 3). To eliminate the activity built up between each tape movement, only data collected during the first proton pulse of each cycle were treated. The resulting decay curves were then unfolded, and the relative activities of the parent and daughter nuclei were extracted.

In this section, we describe the fitting procedure employed to determine the number of decays. The time-dependent release of radioactive ions from a hot target bombarded by high-energy protons may be described by a characteristic release curve [18],

$$P(t) = A(1 - e^{-\lambda_r t})[\alpha e^{-\lambda_f t} + (1 - \alpha)e^{-\lambda_s t}], \qquad (1)$$

where $P(t)$ represents the probability density for an atom generated at $t = 0$ to be released at a given time t. The three parameters λ_r, λ_f, and λ_s are the time constants associated with the effusion, fast diffusion, and slow diffusion processes, respectively. The fraction of fast diffusion is given by α, and A is a normalization constant. Considering the radioactive decay constant λ of a given nucleus, one can define the associated radioactive beam current $i(t)$ by

$$i(t) = c \times P(t) \times e^{-\lambda t}, \qquad (2)$$

where c is related to the number of extracted ions. The evolution of the total number $N(t)$ of implanted ions on the Mylar tape is then governed by the differential equation

$$\frac{dN(t)}{dt} = i(t) - \lambda N(t), \qquad (3)$$

and the measured β activity $D(t)$ of a given isotope at time t is simply given by

$$D(t) = \lambda N(t). \qquad (4)$$

In the following, we consider the specific case of the β decay of ^{52}K. To fully describe the activity measured, one must take into account the complete decay chains. Here, considering the measurement time T_m and the different half-lives, only the K and Ca activities, including the A-1 and A-2 Ca activites after delayed neutron emission, needed to be included. The

TABLE I. Summary of the measurement cycles for each K isotope produced in the experiment. N_p is the number of proton pulses incident the ISOLDE target per supercyle.

Nucleus	N_p	T_d (ms)	T_c (ms)	T_m (ms)	T_{acq} (min)
^{51}K	6	5	1000	2000	180
^{52}K	6	5	600	2000	1500
^{53}K	10	10	500	1000	160

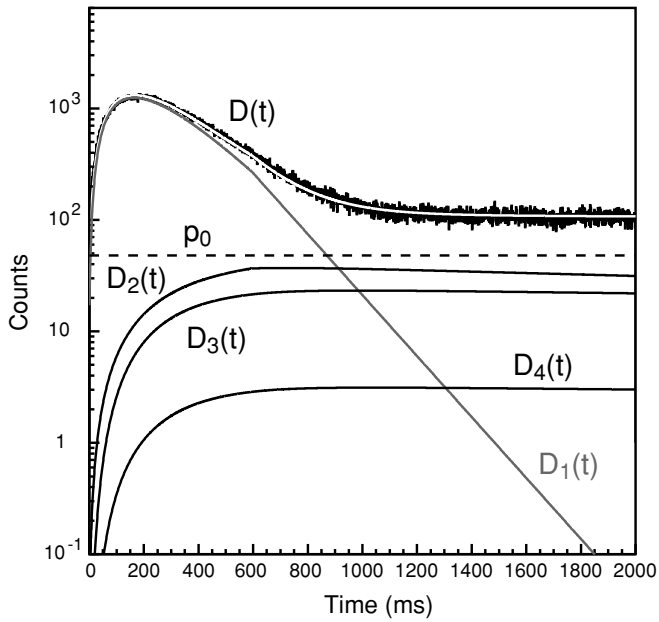

FIG. 3. Radioactive decay activity for ^{52}K for events collected for 2 s after the first proton pulse of each cycle. $D_1(t)$, $D_2(t)$, $D_3(t)$, and $D_4(t)$ correspond to the ^{52}K, ^{52}Ca, ^{51}Ca, and ^{50}Ca activities, respectively (see text). Dotted line shows the constant background. Total activity $D(t)$ is the sum of all these contributions.

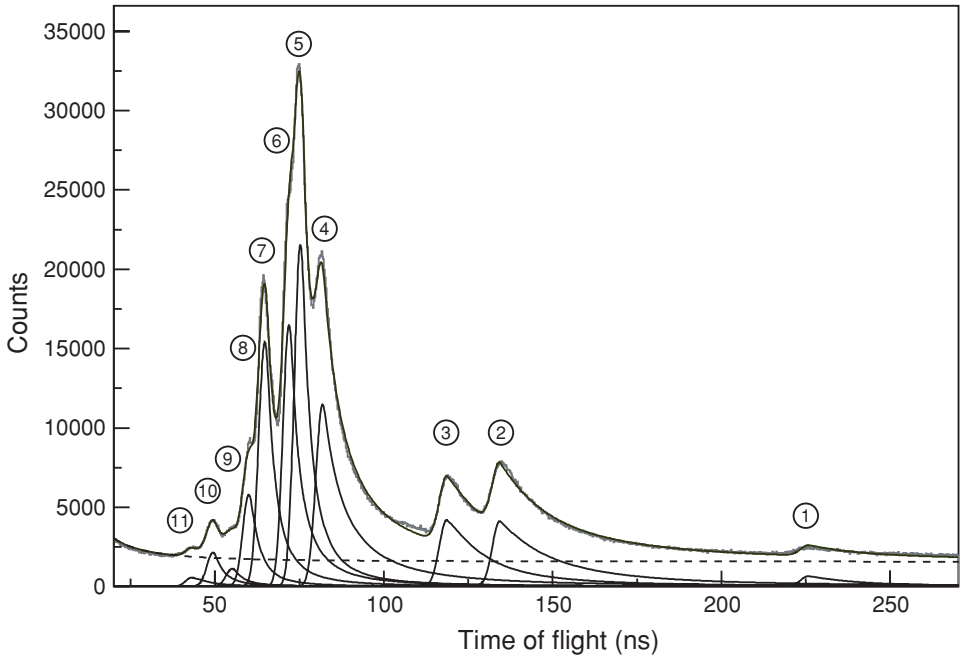

FIG. 4. Time-of-flight spectrum measured with the TONNERRE array for the ^{49}K β-delayed neutron activity. Solid lines represent the fits to the 11 known neutron transitions. Dashed line corresponds to the background arising from the detection of cosmic rays and room background activity.

subsequent activities (i.e., Sc and Ti) were not considered because of their relatively long half-lives. The total activity during the collection time T_c could be described by

$$\begin{cases} \frac{dN_1(t)}{dt} = i_1(t) - \lambda_1 N_1(t), \\ \frac{dN_2(t)}{dt} = i_2(t) - \lambda_2 N_2(t) + \mathbf{P}_{0n} \times \lambda_1 N_1(t), \\ \frac{dN_3(t)}{dt} = \quad - \lambda_3 N_3(t) + \mathbf{P}_{1n} \times \lambda_1 N_1(t), \\ \frac{dN_4(t)}{dt} = \quad - \lambda_4 N_4(t) + \mathbf{P}_{2n} \times \lambda_1 N_1(t), \end{cases} \tag{5}$$

where λ_1, λ_2, λ_3, and λ_4 are the decay constants of ^{52}K, ^{52}Ca, ^{51}Ca, and ^{50}Ca, respectively; P_{1n} and P_{2n} are the $1n$- and $2n$-delayed emission probabilities, and $i_2(t)$ represents the production intensity of the isobaric ^{52}Ca contamination. For $t > T_c$, $i_1(t) = i_2(t) = 0$. The total activity $D(t)$ measured on the tape is

$$D(t) = \sum_{i=1}^{4} D_i(t) + p_0. \tag{6}$$

Each individual activity $D_i(t)$ is analytically obtained from Eqs. (4) and (5). The background component p_0, which arises principally from cosmic rays interacting in the $4\pi\beta$ counter, is constant. A total of nine parameters were used to fit the experimental decay spectrum using Eq. (6). The result is presented in Fig. 3. All four contributions (^{52}K, ^{52}Ca, ^{51}Ca, and ^{50}Ca) were unfolded, and a value of $N_\beta = 4.86(20) \times 10^5$ was extracted for the total number of ^{52}K decays. The uncertainties in the half-lives used in the fit are the main contributions to the error on N_β along with the uncertainty on the constant background level.

In the case of ^{51}K, because the S_{2n} two-neutron separation energy (10 713 keV) is relatively high compared with the estimated Q_β value (13 860 keV) [19], one can consider the delayed $2n$ emission to be very small, if not nonexistent. The last equation therefore disappears from Eq. (5) and only eight parameters are required to fit the experimental decay curve and obtain the ^{51}K, ^{51}Ca, and ^{50}Ca activities. Finally, we obtained $N_\beta = 1.93(5) \times 10^6$ for the total number of ^{51}K decays. A similar eight-parameter fitting procedure was used to obtain the number of ^{53}K decays $N_\beta = 188(30) \times 10^2$.

B. Neutron time-of-flight spectra

We focused our analysis of neutron data on the spectra obtained with the TONNERRE array. They offered much better statistics for performing a quantitative analysis compared to the LEND detectors. In these spectra, the neutron peaks show an asymmetric shape with long tails that extend to lower energies (Fig. 4). These tails arise principally from the delayed fluorescence component of the light produced by the neutrons in the scintillator. A phenomenological parametrization, which consists of three functions, has been used to fit these peaks [20]. A Gaussian shape is used to describe the high-energy tail, a second-order polynomial to describe the peak, and a Lorentzian function for the low-energy tail. A total of 11 parameters is therefore required to reproduce a single peak. However, because the total line shape must be continuous, the description of each neutron peak in the time-of-flight spectrum is reduced to only three free parameters.

Neutron emission probabilities as well as branching ratios require that the neutron detection efficiency ϵ_n be established. As noted above, this was accomplished using a ^{49}K beam. This nucleus has a large neutron emission probability, $P_n = 86(9)\%$ [21], with well-known branching ratios and a wide range of neutron energies (0.15 to 4.86 MeV) [17]. Figure 4 shows the measured ^{49}K time-of-flight spectrum. The intrinsic TONNERRE detection efficiencies deduced from this measurement were in good agreement with previous results [22]: 44.1% at 1.10 MeV and 38.5% at 1.65 MeV. Finally, Monte Carlo simulations [20] performed with the GEANT4 code [23] were used to calculate ϵ_n for all energies up to 5 MeV.

To obtain absolute quantities relative to the total number of β decays N_β, the neutron time-of-flight analyses were carried out using only the data corresponding to the total β-delayed neutron activity after the first proton pulse of each supercycle. After identification in the time-of-flight spectrum of the k most significant neutron contributions, the delayed neutron emission probability P_n was determined using

$$P_n = \frac{1}{N_\beta} \sum_{i=1}^{k} \frac{N_n(E_{n_i})}{\epsilon_n(E_{n_i})}, \tag{7}$$

where E_{n_i} is the energy of the ith transition, and ϵ_n is the total neutron detection efficiency at the energy of the transition.

IV. DECAY OF ^{51}K

A. Results

γ spectroscopy yields information on the low-energy particle-bound levels that are populated in the decay. In this experiment, seven γ transitions have been assigned to the β decay of ^{51}K. They correspond to those observed in the first 1000 ms of each measurement cycle after subtraction of the background and long-lived (>10 s) daughter activities [Fig. 5(a)]. No transitions were observed below 1 MeV. Only the 3460 keV transition is attributed to ^{51}Ca, connecting the first excited state of this nucleus to the ground state. The six remaining transitions have been attributed, through β-γ-n coincidences, to the deexcitation of ^{50}Ca [Fig. 5(b)]. Each level in ^{50}Ca is linked to at least two deexciting transitions or an established cascade. The 2503–1027 γ-γ coincidence allows us to unambiguously locate the 3530 keV state in the level scheme of ^{50}Ca in disagreement with previous results [17]. No known γ transition in ^{49}Ca and ^{49}Sc has been observed indicating that the delayed two-neutron emission probability is very small. The energies and absolute γ intensities of all transitions are listed in Table II. The absolute γ intensities I_γ^{abs} have been determined using

TABLE II. Energies and absolute intensities of γ transitions in ^{50}Ca and ^{51}Ca following the β decay of ^{51}K.

Nucleus	E_γ (keV)	I_γ^{abs} (%)	E_i (keV)	E_f (keV)
^{51}Ca	3460 ± 2	3.9 ± 0.5	3460	0
^{50}Ca	1027 ± 1	21.7 ± 2.2	1027	0
^{50}Ca	1976 ± 1	2.6 ± 0.3	3003	1027
^{50}Ca	2503 ± 1	0.6 ± 0.1	3530	1027
^{50}Ca	3008 ± 2	0.3 ± 0.1	4035	1027
^{50}Ca	3530 ± 2	0.8 ± 0.1	3530	0
^{50}Ca	4035 ± 2	0.5 ± 0.1	4035	0

$$I_\gamma^{\text{abs}} = \frac{N_\gamma}{\epsilon_\gamma \times N_\beta}, \tag{8}$$

where N_γ and N_β are the total numbers of γ rays and β particles, and ϵ_γ is the total γ detection efficiency at the energy of the transition.

Spectroscopy of β-delayed neutrons probes unbound levels in ^{51}Ca. To determine the exact location of levels, we

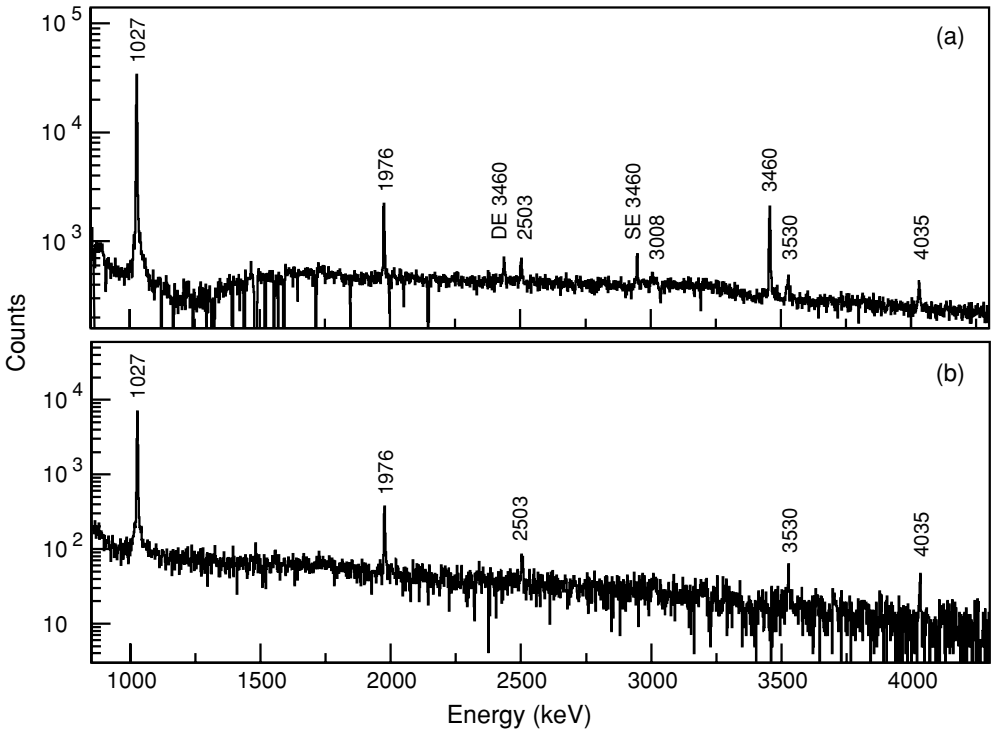

FIG. 5. ^{51}K decay: (a) γ-ray spectrum of activity in the first 1000 ms of each measurement cycle. Data are corrected for background and long-lived (>10 s) daughter activities. Each peak is labeled with the energy of the transition. Peaks SE and DE identify single- and double-escape peaks, respectively. (b) γ-ray spectrum in coincidence with the TONNERRE array.

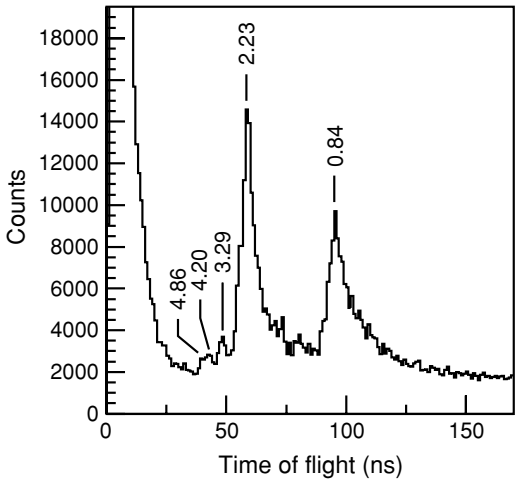

FIG. 6. Time-of-flight spectrum measured with the TONNERRE array corresponding to the feeding of the ^{50}Ca ground state in the decay of ^{51}K. Neutron energies are in MeV.

performed a β-γ-n triple coincidence analysis of the data. The neutron time-of-flight spectrum was gated on the four most intense γ transitions deexciting levels in ^{50}Ca. The resulting γ-gated neutron spectra were corrected for the different contributions arising from the feeding of higher energy levels that afterward deexcite to the "gating" level. We consequently identified 7, 6, 4, and 3 new neutron transitions feeding the levels in ^{50}Ca located at 1027, 3003, 3530, and 4035 keV, respectively. To identify the remaining neutron transitions that feed the ground state of ^{50}Ca, we summed up all the γ-gated neutron spectra and subtracted the resulting spectrum from the total neutron time-of-flight spectrum. Five new neutron transitions have thus been assigned to the decay to the ground state of ^{50}Ca (Fig. 6). In Table III, we list all the energies and relative intensities of the neutron transitions connecting unbound levels in ^{51}Ca to bound levels in ^{50}Ca. Finally, using the 17 most significant neutron peaks identified in the total neutron time-of-flight spectrum (Fig. 7), the delayed neutron

TABLE III. Energies and relative intensities of delayed neutron transitions following the β decay of ^{51}K. For absolute neutron intensities per 100 decays, $I_n^{\rm rel}$ values must be multiplied by 0.218.

E_n (keV)	$I_n^{\rm rel}$ (%)	$E_\gamma^{\rm coinc}$ (keV)	E_f(^{50}Ca) (keV)
820 ± 25	5.5 ± 1.6	1027	1027
910 ± 30	9.2 ± 2.1	1027	1027
1170 ± 40	22.0 ± 3.9	1027	1027
1540 ± 50	21.6 ± 3.9	1027	1027
2190 ± 80	12.4 ± 2.4	1027	1027
3070 ± 130	7.3 ± 1.6	1027	1027
3670 ± 180	5.5 ± 1.5	1027	1027
530 ± 20	0.5 ± 0.2	1976	3003
780 ± 20	2.3 ± 0.7	1976	3003
980 ± 40	4.6 ± 1.0	1976	3003
1470 ± 50	1.4 ± 0.4	1976	3003
1840 ± 120	2.3 ± 0.6	1976	3003
2570 ± 200	0.9 ± 0.3	1976	3003
690 ± 20	1.4 ± 0.5	2503	3530
960 ± 40	1.4 ± 0.4	2503	3530
1460 ± 100	2.3 ± 0.4	2503	3530
2270 ± 120	1.4 ± 0.4	2503	3530
830 ± 20	1.8 ± 0.4	4035	4035
1420 ± 80	0.9 ± 0.3	4035	4035
1990 ± 100	0.9 ± 0.4	4035	4035
840 ± 25	63.1 ± 11.5	–	0
2230 ± 80	100	–	0
3290 ± 150	10.2 ± 2.3	–	0
4200 ± 220	5.1 ± 1.6	–	0
4860 ± 270	5.1 ± 1.7	–	0

emission probability P_n was determined using Eq. (7). The result yields $P_n = P_{1n} = 63 \pm 8\%$, which is in very good agreement with the value of $68 \pm 10\%$ reported by Langevin *et al*. [24] and clearly in conflict with the first $P_n = 47 \pm 5\%$ value originally obtained by Carraz *et al*. [21].

The absolute β-branching ratios to the neutron-emitting states were obtained by normalizing the total intensity of the

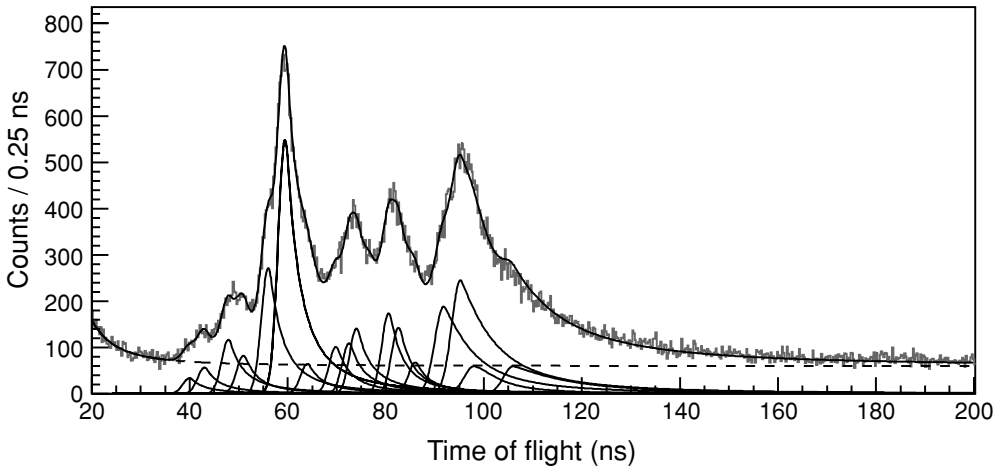

FIG. 7. Time-of-flight spectrum measured with the TONNERRE array from the ^{51}K β-delayed neutron activity after the first proton pulse of each supercycle. Solid lines represent fits to the 17 most significant individual neutron transitions. Dashed line corresponds to the background.

neutron lines to the $1n$-emission probability P_{1n} (see above). More precisely, relative feedings in ^{50}Ca were determined from the difference between the γ feeding and γ decay of each excited level. Absolute $I_{\beta n}$ values were then obtained using the total number of decays N_β deduced from the analysis of the time spectrum (Sec. III A). The total neutron feeding to the four excited states observed in ^{50}Ca amounts to $23.0 \pm 2.5\%$ of the decays. Subtracting this from P_{1n} yields the value $I_{\beta n_0} = 40 \pm 8\%$ for the neutron feeding to the ground state of ^{50}Ca. From these results, and using the relative neutron intensities quoted in Table III, we were able to calculate the feeding I_β to each individual state in ^{51}Ca. Finally, a reliable estimate of the β transition to the ground state of ^{51}Ca was obtained from the delayed one-neutron emission probability P_{1n} and the feeding to the first excited state of ^{51}Ca. Summing up the two contributions yields $I_{\beta_0} = 33.1 \pm 8.0\%$.

The β-branching ratios, log (base 10) f_0t values, and corresponding reduced transition probabilities B(GT) to the levels in ^{51}Ca populated in the β decay of ^{51}K are listed in Table IV. The excitation energies of the unbound levels in ^{51}Ca were calculated taking into account the recoil energy of the final nucleus and a neutron separation energy equal to 4360 ± 90 keV [19]. The log f_0t values were calculated with $T_{1/2} = 365 \pm 5$ ms [24] and using the mass values of Audi *et al.* [19]. The Gamow-Teller strength B(GT) as a function of the excitation energy in the daughter nucleus was calculated using

$$B(\mathrm{GT}) = \frac{K I_\beta}{f(Q_\beta - E_x)T_{1/2}}, \tag{9}$$

TABLE IV. β branching, log (base 10), f_0t, and B(GT) values in the decay of ^{51}K to bound and unbound levels in ^{51}Ca. B(GT) values are in units of $g_A^2/4\pi$. Levels marked with asterisk correspond to two or three closely spaced levels; log f_1t values for the ground and 3.46 MeV states are 8.7 ± 0.1 and 8.8 ± 0.2, respectively.

E_x (keV)	I_β (%)	log f_0t	B(GT) $\times 10^5$
0	33.1 ± 8.0	6.0 ± 0.1	380 ± 65
3460 ± 2	3.9 ± 0.5	6.4 ± 0.1	175 ± 50
5220 ± 20	13.8 ± 1.8	5.4 ± 0.2	1480 ± 515
6220 ± 25	1.2 ± 0.3	6.2 ± 0.3	203 ± 105
6320 ± 30	2.0 ± 0.4	6.0 ± 0.2	425 ± 175
6600 ± 50*	26.6 ± 3.4	4.8 ± 0.2	6440 ± 2410
6960 ± 50	4.7 ± 0.6	5.4 ± 0.2	1435 ± 560
7650 ± 100*	5.0 ± 0.8	5.2 ± 0.2	2430 ± 1065
7900 ± 20	0.10 ± 0.05	6.8 ± 0.4	60 ± 40
8160 ± 20	0.5 ± 0.1	6.0 ± 0.3	370 ± 175
8360 ± 40	1.0 ± 0.3	5.6 ± 0.3	865 ± 470
8590 ± 100*	2.9 ± 0.7	5.1 ± 0.3	3050 ± 1470
8870 ± 60*	0.6 ± 0.2	5.7 ± 0.3	810 ± 430
9130 ± 120	1.2 ± 0.3	5.3 ± 0.3	2060 ± 1125
9240 ± 60*	0.9 ± 0.2	5.4 ± 0.3	1720 ± 920
9360 ± 150*	1.6 ± 0.4	5.1 ± 0.4	3440 ± 1910
9880 ± 130*	0.4 ± 0.1	5.4 ± 0.4	1490 ± 865
10210 ± 120	0.3 ± 0.1	5.4 ± 0.5	1640 ± 1060
10420 ± 100	0.2 ± 0.1	5.4 ± 0.4	1410 ± 870

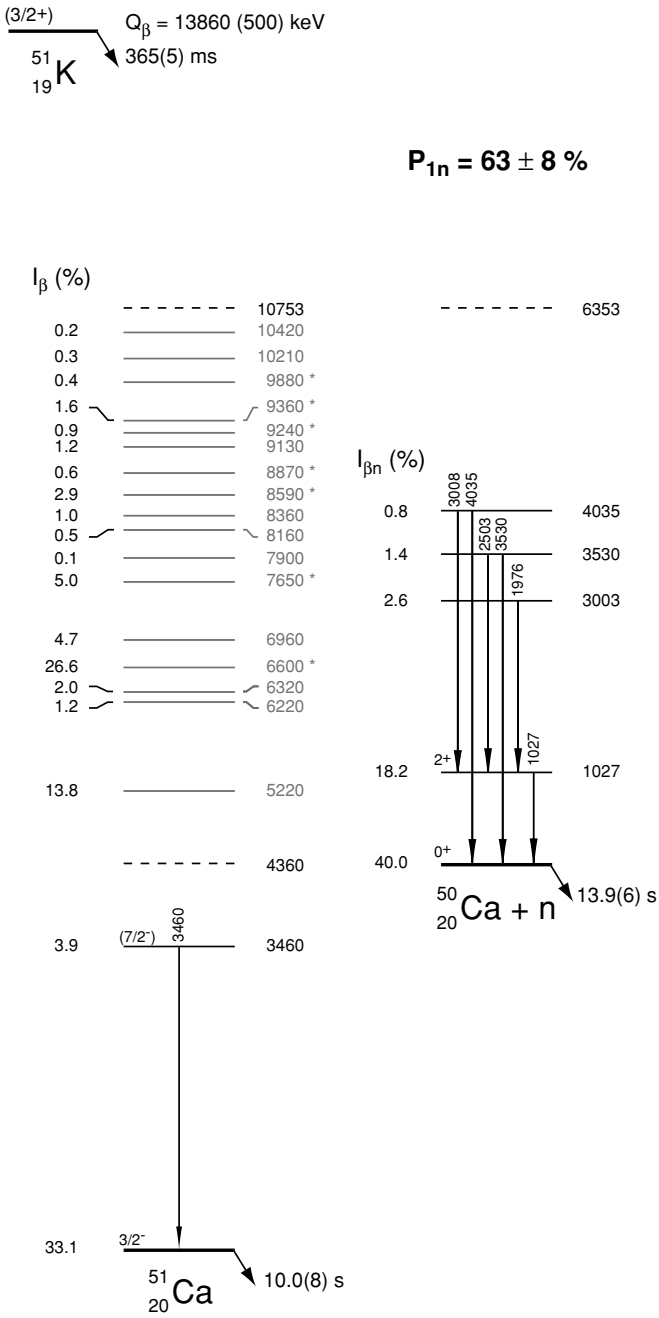

FIG. 8. Proposed decay scheme for ^{51}K. Dashed lines indicate the neutron emission thresholds in ^{51}Ca and ^{50}Ca. Unbound levels marked by * correspond to two or three closely spaced levels.

where I_β is the β branching to a level with an excitation energy of E_x, $f(Q_\beta - E_x)$ is the integral of the Fermi function, $T_{1/2}$ is the β-decay half-life in seconds, and $K = 3833 \pm 24$ s [25, 26]. The established ^{51}K decay scheme to particle-bound and particle-unbound states in ^{51}Ca is presented in Fig. 8.

B. Discussion

One should first note that the ^{51}K decay data available in the literature [17] are based on experiments that failed to

detect significant fragmented strength at high excitation energy in the daughter nucleus. This led to large systematic errors, especially in the determination of the β-branching ratios. In addition, the reported β intensities have been normalized using the very low P_n value of Carraz and coworkers [21], resulting in large discrepancies with respect to our results, especially for the branching ratios to the ground and first excited states of ^{51}Ca. It should be stressed that here all the relevant quantities were measured in a single experiment, and the absolute γ and neutron intensities were thus obtained in a consistent way using, as opposed to earlier experiments, the total number of decays N_β.

There is currently no experimental determination of the spin and parity of the ground state of ^{51}K. Shell-model calculations suggest $J^\pi = 1/2^+$ or $3/2^+$ depending on the degeneracy of the two $\pi s_{1/2}$ and $\pi d_{3/2}$ orbitals as the occupation of the $\nu p_{3/2}$ shell increases [27]. The behavior of the $1/2^+$-$3/2^+$ doublet along the odd-A K isotopes is experimentally known up to $N = 28$ with the $1/2^+$ state becoming the ground state for ^{47}K [28,29]. Shell-model predictions for higher mass K isotopes depend strongly on which effective interaction is used for the calculations, and it is not yet clear if the $\pi s_{1/2}$-$\pi d_{3/2}$ inversion persists for ^{51}K [27,30]. The ground state of ^{50}K has been shown to have $J^\pi = 0^-$, corresponding to a $(\pi d_{3/2})^{-1} \otimes (\nu p_{3/2})^3$ configuration [31,32]. This is a strong indication of the reordering of the $\pi s_{1/2}$ and $\pi d_{3/2}$ orbitals above $N = 28$. This suggests that the ^{51}K ground state could have $J^\pi = 3/2^+$ with the $\nu p_{3/2}$ shell filled and a proton hole in the $\pi d_{3/2}$ orbital. In that case, the allowed Gamow-Teller transitions ($\Delta J = 0$, and no parity change) would feed nonnatural parity states with $J^\pi = 1/2^+, 3/2^+$, or $5/2^+$, whereas first-forbidden transitions ($\Delta J = 0, 1, 2$ and parity change) would feed negative parity states with spins between 1/2 and 7/2.

The spin and parity of the ground state of ^{51}Ca has not been experimentally determined. However, if one considers that ^{52}Ca may well exhibit a particularly strong $N = 32$ subshell closure, it is very likely that ^{51}Ca has a $3/2^-$ ground state corresponding to a $(f_{7/2})^8 \otimes (p_{3/2})^3$ neutron configuration. Only one excited state, located at 3.46 MeV, is observed above the ground state of ^{51}Ca. Considering that the first nonnatural parity state in ^{49}Ca, within reach of β decay, is located at 4.27 MeV [33,34], it is possible that the 3.46 MeV state in ^{51}Ca is also of nonnatural parity. A log $f_0 t = 6.4$ could be compatible with the assumption of an allowed transition. However, the relatively strong $N = 32$ subshell closure [8] privileges a dominant $(\nu f_{7/2})^8 \otimes (\nu p_{3/2})^4$ configuration for ^{51}K, and the transformation of a neutron in the $\nu f_{7/2}$ or $\nu p_{3/2}$ orbitals seem to be favored, feeding either the $3/2^-$ ground state or a $7/2^-$ excited state in ^{51}Ca (Fig. 9). This picture is supported by the large feeding $I_{\beta_0} = 33.1\%$ to the ^{51}Ca ground state, while the high excitation energy of the possible $7/2^-$ state at 3.46 MeV could be consistent with the strong binding of the $\nu f_{7/2}$ orbital (i.e., a large gap at the $N = 28$ shell closure). Therefore, it is not surprising to observe no populated states below 3 MeV in an even-odd nucleus, such as the $1/2^-$ state in ^{49}Ca located at 2.02 MeV [35]. In fact, these states have a $(p_{3/2})^2 \otimes (p_{1/2})^1$ neutron configuration, which is very difficult to feed starting from an almost pure $\nu p_{3/2}{}^4$ ground state configuration in ^{51}K.

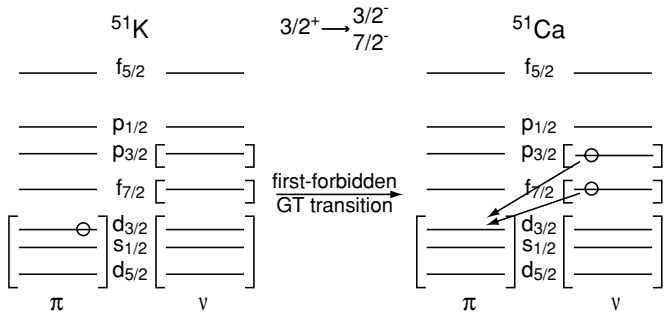

FIG. 9. Left: configuration of the $3/2^+$ ground state in ^{51}K. Right: configurations of the $3/2^-$ and $7/2^-$ excited states in ^{51}Ca, which correspond to the transformation of a $\nu p_{3/2}$ or $\nu f_{7/2}$ neutron into a $\pi d_{3/2}$ proton.

V. DECAY OF ^{52}K

A. Results

Figure 10 shows the decay curve for β particles in coincidence with 2563 keV γ rays in ^{52}Ca. The curve was fitted from 600 to 2000 ms (beam gate closed) with a single exponential decay and a constant background. The extracted half-life $T_{1/2} = 118 \pm 6$ ms is in good agreement with the previous measurements of 105 ± 5 [24] and 110 ± 30 ms [8].

Figure 11(a) presents the β-delayed γ-ray spectrum that shows the transitions observed in the first 1000 ms of each measurement cycle after subtraction of the background and long-lived (>4 s) daughter activities. In addition to the known 2563 keV transition in ^{52}Ca [8], ten new γ transitions were observed and assigned to the β decay of ^{52}K. Among these transitions, six are seen in coincidence with delayed neutrons [Fig. 11(b)].

The triple γ-γ coincidences between the 1427, 1961 keV and the known 2563 keV transitions allowed us to

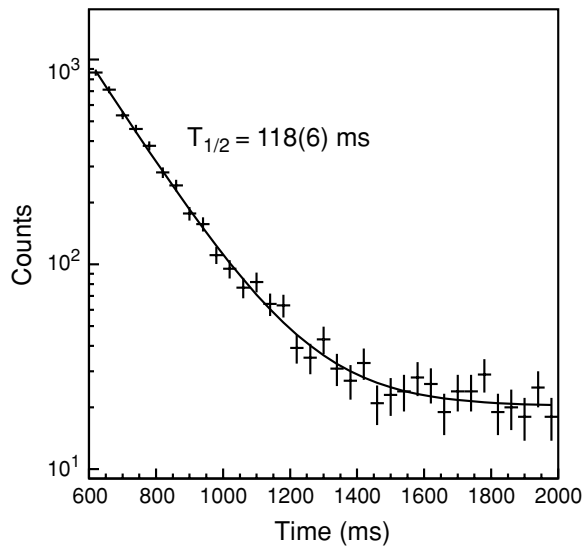

FIG. 10. Decay curve for ^{52}K in coincidence with the intense 2563 keV γ transition in ^{52}Ca. Data were fitted with a single exponential and constant background.

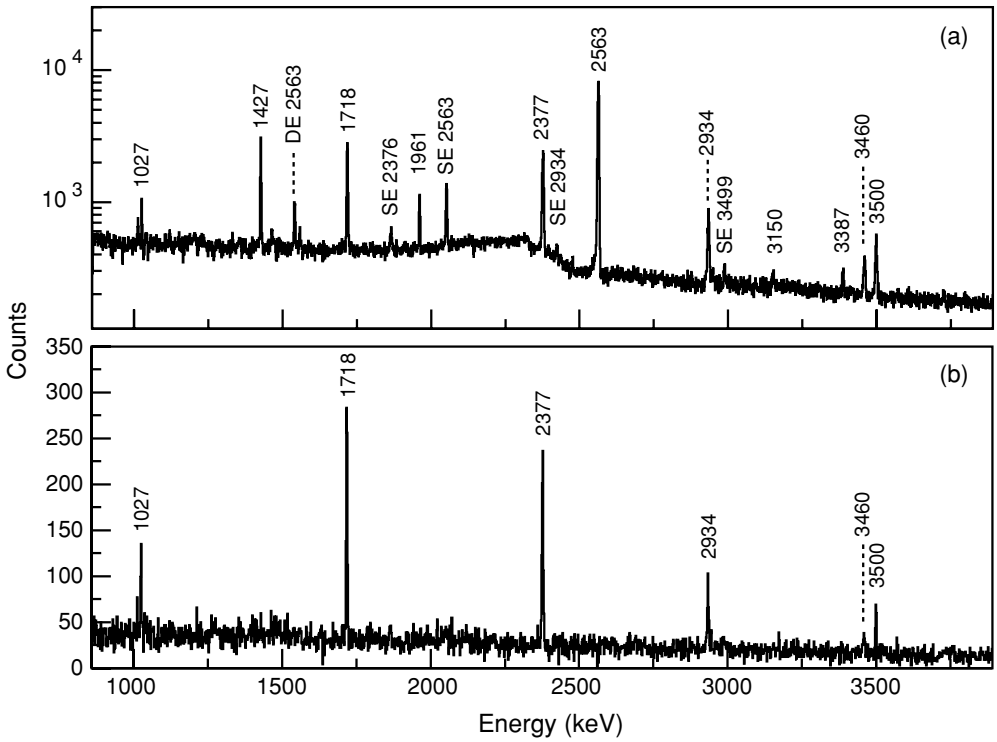

FIG. 11. ^{52}K decay: (a) γ-ray spectrum of activity in the first 1000 ms of each measurement cycle. Data are corrected for background and long-lived (>4 s) daughter activities. (b) γ-ray spectrum in coincidence with β-delayed neutrons detected by the TONNERRE array. Labels are the same as in Fig. 5.

unambiguously locate two new states in the level scheme of ^{52}Ca at 3990 and 5951 keV excitation energy. An additional but very weak 2563–3388 γ-γ coincidence confirms the presence of the 5951 keV state, above the one-neutron emission threshold ($S_{1n} = 4700$ keV). The remaining 3150 keV transition, seen only in the direct spectrum, is assigned to the γ decay of a new level at this excitation energy.

To assign the γ transitions seen in coincidence with neutrons, it is interesting to note that for the $2n$-γ events, the overall efficiency is increased owing to the presence of two neutrons. Indeed, if we compare the ratios of γ intensities measured for β-γ-n and β-γ coincidences (Fig. 12), we note that the values obtained for the transitions related to the $1n$ process are smaller than that for the 1027 keV line. From the figure, it appears clearly that the 1718, 2377, 2934, 3460, and 3500 keV transitions may be attributed to levels in ^{51}Ca. The 1718, 3460, and 3500 keV transitions are not seen in coincidence with any other γ rays and are therefore assumed to deexcite levels located at these energies. The 2377 keV γ ray is seen in coincidence with a less intense 1123 keV transition, thus confirming the placement of the 3500 keV state. Finally, an additional 2934–1159 coincidence allows us to place a sixth level in ^{51}Ca at 4493 keV. The energies and absolute γ intensities of all transitions are listed in Table V. The absolute γ

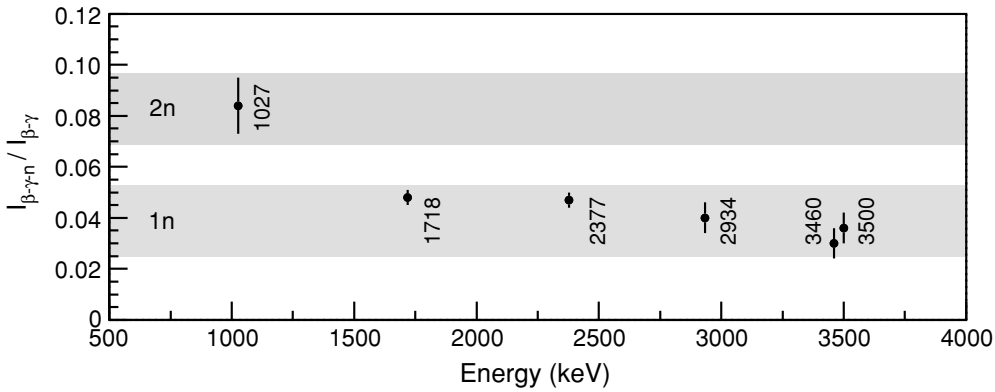

FIG. 12. Intensity ratio $I_{\beta\text{-}\gamma\text{-}n}/I_{\beta\text{-}\gamma}$ of the γ lines in coincidence with neutrons and only with β particles. Note the two groups of transitions related to $1n$ and $2n$ decays (see text).

TABLE V. Energies and absolute intensities of γ transitions in ^{50}Ca, ^{51}Ca, and ^{52}Ca following the β decay of ^{52}K.

Nucleus	E_γ (keV)	$I_\gamma^{\rm abs}$ (%)	E_i (keV)	E_f (keV)
^{52}Ca	1427 ± 1	4.4 ± 0.4	3990	2563
^{52}Ca	1961 ± 1	1.5 ± 0.2	5951	3990
^{52}Ca	2563 ± 1	25.2 ± 2.5	2563	0
^{52}Ca	3150 ± 2	0.30 ± 0.05	3150	0
^{52}Ca	3388 ± 2	0.40 ± 0.06	5951	2563
^{51}Ca	1123 ± 1	0.20 ± 0.04	3500	2377
^{51}Ca	1559 ± 1	0.40 ± 0.05	4493	2934
^{51}Ca	1718 ± 1	5.4 ± 0.5	1718	0
^{51}Ca	2377 ± 1	6.9 ± 0.7	2377	0
^{51}Ca	2934 ± 1	3.0 ± 0.3	2934	0
^{51}Ca	3460 ± 2	1.10 ± 0.15	3460	0
^{51}Ca	3500 ± 2	1.9 ± 0.2	3500	0
^{50}Ca	1027 ± 1	0.55 ± 0.06	1027	0

intensities $I_\gamma^{\rm abs}$ were determined using Eq. (8) and the absolute ^{52}K activity (Sec. III A).

In the case of ^{52}K, the emission of one and two neutrons is observed through the related γ activities. Indeed, the observation of the 1027 keV transition deexciting the 2_1^+ excited state of ^{50}Ca signals unambiguously the delayed two-neutron emission. To our knowledge, this is the first evidence for the population of an excited state in $2n$ emission following the decay of a neutron-rich potassium isotope. Considering the 15 most significant neutron lines identified in the time-of-flight spectrum (Fig. 13) and using Eq. (7), we derived $P_n = 79 \pm 12\%$ for ^{52}K. This results is compatible with the $P_n = 107 \pm 20\%$ reported by Langevin *et al*. [24]. To disentangle the $1n$ and $2n$ contributions, one has to solve the following equations:

$$\begin{aligned} P_{1n} + P_{2n} &= 1 - I_\gamma - I_{\beta_0}, \\ P_{1n} + 2P_{2n} &= P_n, \end{aligned} \tag{10}$$

where I_{β_0} and I_γ are the feedings to the ground and excited states of ^{52}Ca, respectively. Unfortunately, as the ^{52}Ca ground state feeding is also unknown, one needs an additional relationship between P_{1n} and P_{2n} in order to solve the problem.

From the intensities of the principal γ transitions in ^{51}Sc and ^{50}Sc, the total number of ^{51}Ca and ^{50}Ca decays could be precisely determined, yielding a relative activity $N_\beta(^{51}\text{Ca})/N_\beta(^{50}\text{Ca})$ of 42 ± 5. Using our parametrization of the time evolution of the ion implantation and decay (Sec. III A), we varied iteratively the P_{1n} and P_{2n} values in order to match the experimental ratio of the ^{51}Ca and ^{50}Ca activities. This fine-tuning procedure yielded a ratio of $P_{1n}/P_{2n} = 32 \pm 4$. With this result, one can solve (10). Finally, we obtained $P_{1n} = 74.4 \pm 9.3\%$, $P_{2n} = 2.3 \pm 0.3\%$, and an upper limit of 8% for I_{β_0}.

The time-of-flight spectra of the delayed neutrons measured with the TONNERRE and LEND detectors are shown in Fig. 14. The structures observed at high energy ($E_n >$ 1.5 MeV) are in relatively good agreement with the ones previously measured by Huck *et al*. [8]. The low neutron detection threshold available in the present experiment allowed us to clearly identify the transition at 1.03 MeV as well as additional transitions with energies as low as 200 keV.

To locate the unbound levels in ^{52}Ca, we performed a β-γ-n triple coincidence analysis of the data. The total neutron time-of-flight spectrum was gated by the different γ transitions deexciting the levels in ^{51}Ca. Figure 15 shows the neutron spectra gated by the two most intense γ transitions corresponding to the feeding of the 1718 and 2377 keV states. In a similar way, we identified neutron transitions in coincidence with the 2934, 3460, and 3500 keV γ lines in ^{51}Ca. As the 1559 keV γ transition was too weak, there were not sufficient statistics to analyze the gated time-of-flight spectrum and determine the transitions feeding the 4493 keV state in ^{51}Ca. To identify the remaining neutron transitions that feed the ground state of ^{51}Ca we summed up all the γ-gated spectra after having corrected each one for the appropriate γ detection efficiency. The resulting spectrum was then subtracted from the total neutron time-of-flight spectrum, and seven neutron

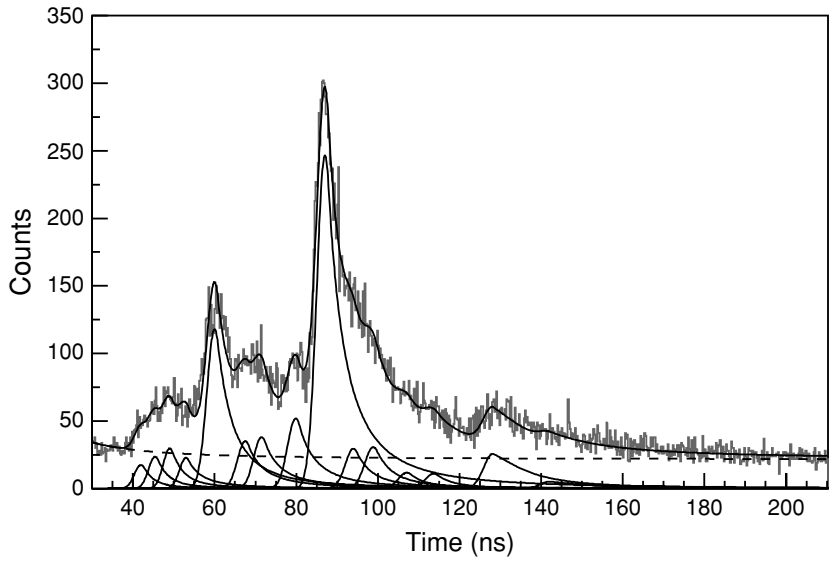

FIG. 13. Same as Fig. 7, but for ^{52}K. Solid lines represent fits to the 15 most significant neutron transitions.

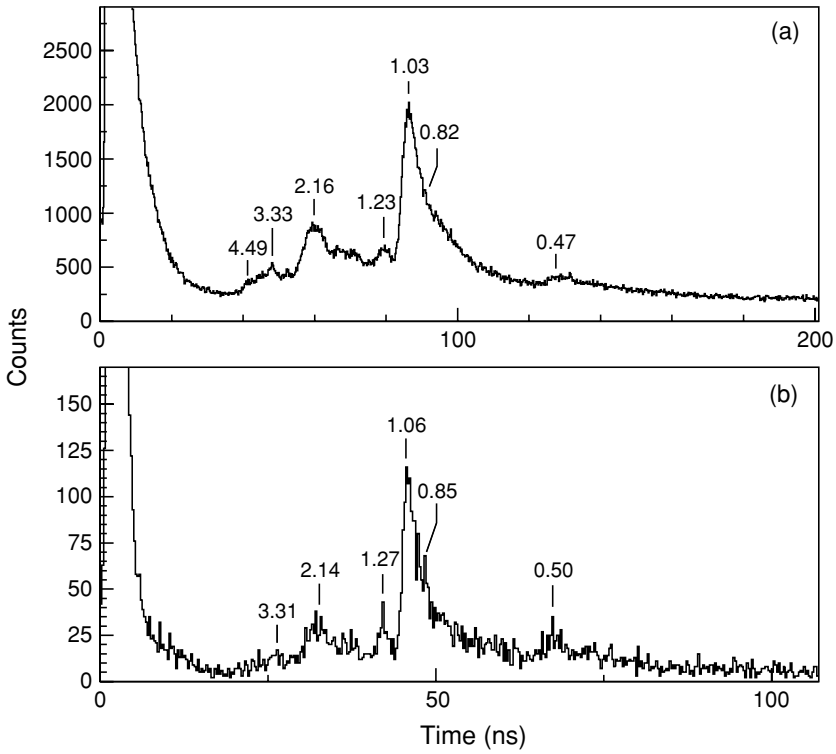

FIG. 14. Delayed neutron spectra measured with the (a) TONNERRE and (b) LEND arrays from the ^{52}K β-delayed neutron activity. Neutron energies are in MeV.

transitions were assigned to the decay process to the ground state of ^{51}Ca (Fig. 16). In Table VI, we list all the energies and relative intensities of the neutron transitions connecting unbound levels in ^{52}Ca to bound levels in ^{51}Ca. Note that the energies result from the observation of maxima in the time-of-flight neutron spectrum and may in some cases correspond to several unresolved states.

Table VII gives the absolute neutron feedings to the levels in ^{51}Ca and ^{50}Ca. Relative feedings were determined first from the γ imbalances, and then absolute $I_{\beta n}$ values were obtained using the total number of ^{52}K decays deduced from the analysis of the time spectrum. The total neutron feeding to the six excited states observed in ^{51}Ca amounts to $18.3 \pm 1.0\%$ which, when combined with the P_{1n}, yields $I_{\beta n_0} = 56.1 \pm 9.4\%$ for the neutron feeding to the ground state of ^{51}Ca. In a similar way, using the intensity of the 1027 keV γ line and the P_{2n} value, a neutron feeding to the ground state of ^{50}Ca was found to be $I_{\beta 2n_0} = 1.8 \pm 0.3\%$. From these results, and using the relative neutron intensities listed in Table VI, we were able to calculate the feeding I_β to each individual state in ^{52}Ca.

The β-branching ratios, log $f_0 t$ values, and corresponding reduced transition probabilities B(GT) to the levels in ^{52}Ca populated in the β decay of ^{52}K are tabulated in Table VIII. The excitation energies of the unbound levels in ^{52}Ca were calculated as done for ^{51}K, but with a neutron separation energy of 4700 ± 700 keV [19]. The log $f_0 t$ values were calculated with $T_{1/2} = 118 \pm 6$ ms and, using the Q_β evaluation of Audi *et al.* [19]. B(GT) was again calculated using Eq. (9). The absolute β-branching ratios to the neutron-emitting states were obtained by normalizing the total intensity of the neutron lines to the $P_{1n} + P_{2n}$ value. Because low-lying levels in ^{52}Ca are expected to be mainly natural parity states fed by first-forbidden transitions, we also give in Table VIII the log $f_1 t$ values for the bound states in ^{52}Ca.

The decay scheme of ^{52}K established on the basis of our β-γ-γ and β-n-γ coincidence analysis (Fig. 17) gives an extended description of the neutron-emitting states in ^{52}Ca, if one takes for granted the zero feeding of the ^{52}Ca ground state.

B. Discussion

We have determined from the combined γ and neutron analyses that the feeding I_{β_0} to the ground state of ^{52}Ca is lower than 8%. This is in contrast to the decays of ^{50}K and ^{51}K for which I_{β_0} values of 61.0% [32] and 33.1% (Sec. IV A) were determined, respectively. A $0^- \rightarrow 0^+$ transition would be strongly enhanced by a meson-exchange current such as observed in the decay of ^{50}K [32]. The absence of such a strong transition in the present case seems to rule out a 0^- assignment for the ^{52}K ground state. In addition, the log $f_1 t = 8.4$ value for the transition to the 2^+ state in ^{52}Ca is not compatible with a 0^- assignment for the ^{52}K ground state. Indeed, the systematic classification of the Gamow-Teller first-forbidden transitions [36] shows that unique first-forbidden transitions (with $\Delta J = 2$) have log $f_1 t$ values greater than 8.5. The corresponding wave function must therefore have a proton hole in the $d_{3/2}$ orbital that couples to a $p_{1/2}$ valence neutron to give a 1^- or 2^- ground state for ^{52}K. The very weak feeding of the ^{52}Ca ground state suggests a forbidden transition with a relatively high ($\Delta J = 2$) momentum transfer. In this picture, the ^{52}K ground state could be $J^\pi = 2^-$, and the allowed

TABLE VI. Same as Table III, but for the β decay of ^{52}K. $I_n^{\rm rel}$ values must be multiplied by 0.216.

E_n (keV)	$I_n^{\rm rel}$ (%)	$E_\gamma^{\rm coinc}$ (keV)	$E_f(^{51}\mathrm{Ca})$ (keV)
240 ± 5	2.3 ± 0.7	1718	1718
330 ± 30	1.9 ± 0.6	1718	1718
510 ± 15	1.9 ± 0.6	1718	1718
730 ± 20	3.2 ± 0.8	1718	1718
1130 ± 35	4.6 ± 1.1	1718	1718
1930 ± 90	10.2 ± 2.4	1718	1718
3600 ± 200	1.4 ± 0.4	1718	1718
280 ± 10	2.8 ± 0.9	2377	2377
380 ± 10	2.8 ± 0.9	2377	2377
990 ± 20	12.0 ± 2.4	2377	2377
1260 ± 40	3.7 ± 0.9	2377	2377
1600 ± 80	5.1 ± 1.1	2377	2377
2270 ± 120	2.3 ± 0.6	2377	2377
3050 ± 250	2.3 ± 0.7	2377	2377
880–980	4.6 ± 1.2	2934	2934
1250–1480	4.2 ± 1.1	2934	2934
1960 ± 70	3.2 ± 0.9	2934	2934
950 ± 40	1.9 ± 0.6	3460	3460
1380 ± 80	1.9 ± 0.5	3460	3460
2370–3390	1.4 ± 0.4	3460	3460
580–880	6.9 ± 2.1	3500	3500
2260 ± 150	2.8 ± 0.9	3500	3500
480 ± 20	19.9 ± 5.0	–	0
830 ± 30	30.2 ± 7.4	–	0
1040 ± 40	100	–	0
1230 ± 40	14.2 ± 3.8	–	0
2220 ± 80	55.8 ± 15.3	–	0
3520 ± 120	21.4 ± 6.0	–	0
4600 ± 210	7.8 ± 2.3	–	0

Gamow-Teller transitions ($\Delta J = 0, 1$ and no parity change) would feed nonnatural parity states with $J^\pi = 1^-, 2^-$, or 3^-, whereas first-forbidden transitions ($\Delta J = 0, 1, 2$ and parity change) would feed positive parity states with spins between 0 and 4.

The state located at 2563 keV is known to be the first 2^+ excited state [8]. For states at higher excitation energies, the spins and parities have not yet been experimentally determined. The 3150 keV level could correspond to the first nonnatural parity state. However, the log f_0t and log f_1t values suggest a first-forbidden transition to a natural parity state. In addition, if the 3150 keV state was the first nonnatural parity state (3^- for even Ca isotopes with A between 42 and 48), we would expect a strong γ transition connecting this state to the 2_1^+ state as observed in ^{44}Ca and ^{48}Ca. Instead, we observe only a transition to the 0^+ ground state. Therefore, it is very likely that the 3150 keV level is of natural parity with $J^\pi = 1^+$ or 2^+. A 0^+ state could only decay to the ground state by electron conversion, and the transition would not be observed in the γ spectrum. Furthermore, $3^+ \rightarrow 0^+(M3)$ and $4^+ \rightarrow 0^+(E4)$ transitions are very improbable.

Deriving the spin and parity of the 3990 keV level is not straightforward. It could be the first nonnatural parity state with $J^\pi = 3^-$, the corresponding log f_0t value being compatible with an allowed Gamow-Teller transition. We expect in that case a strong transition between this and the 2_1^+ state as experimentally observed with the 1427 keV γ ray. Nevertheless, the possibility of a natural parity state remains with a log f_1t value compatible with a $\Delta J = 0$, 1 or 2 first-forbidden transition. As this state is not directly connected to the ground state of ^{52}Ca, the 0^+, 3^+, and 4^+ assignments in that case are the most likely, although $J^\pi = 1^+$ or 2^+ are not excluded.

TABLE VII. Intensities of one- and two-neutron emissions from unbound levels in ^{52}Ca populated in the β decay of ^{52}K as deduced from γ-intensity analyses (see text). $P_{1n} = 72.2 \pm 9.3\%$ and $P_{2n} = 2.3 \pm 0.3\%$.

E_x (^{51}Ca) (keV)	$I_{\beta n}$ (%)	E_x (^{50}Ca) (keV)	$I_{\beta 2n}$ (%)
0	56.1 ± 9.4	0	1.8 ± 0.3
1718	5.4 ± 0.5	1027	0.5 ± 0.1
2377	6.7 ± 0.7		
2934	2.6 ± 0.3		
3460	1.1 ± 0.2		
3500	2.1 ± 0.2		
4493	0.4 ± 0.1		

TABLE VIII. Same as Table IV, but for the decay of ^{52}K to levels in ^{52}Ca. Log (base 10) f_1t values for the 2563, 3150, 3990, and 5951 keV states are 8.4 ± 0.2, 10.1 ± 0.2, 8.9 ± 0.2, and 8.6 ± 0.3, respectively.

E_x (keV)	I_β (%)	log f_0t	B(GT) $\times 10^5$
0	0	–	–
2563 ± 1	20.4 ± 2.3	5.7 ± 0.2	775 ± 305
3150 ± 2	0.3 ± 0.1	7.3 ± 0.3	14 ± 8
3990 ± 2	2.9 ± 0.3	6.3 ± 0.1	185 ± 75
5190 ± 20	4.3 ± 0.8	5.9 ± 0.3	450 ± 215
5550 ± 30	6.5 ± 1.1	5.7 ± 0.3	790 ± 380
5760 ± 40	21.6 ± 3.8	5.1 ± 0.3	2890 ± 1415
5950 ± 40	3.1 ± 0.6	5.9 ± 0.3	450 ± 245
5951 ± 2	1.9 ± 0.2	6.2 ± 0.2	275 ± 120
$6700 \pm 50^*$	0.9 ± 0.1	6.6 ± 0.3	185 ± 100
$6940 \pm 80^*$	12.5 ± 2.6	5.1 ± 0.3	2930 ± 1570
7160 ± 20	0.7 ± 0.1	6.3 ± 0.3	185 ± 95
$7410 \pm 50^*$	1.2 ± 0.1	6.3 ± 0.3	360 ± 205
7570 ± 35	1.1 ± 0.2	6.0 ± 0.3	355 ± 190
8090 ± 20	2.6 ± 0.3	5.5 ± 0.3	1170 ± 605
8290 ± 120	4.6 ± 1.0	5.2 ± 0.4	2235 ± 1290
$8370 \pm 80^*$	3.0 ± 0.8	5.2 ± 0.4	1530 ± 880
8530–8630	1.1 ± 0.2	5.8 ± 0.4	635 ± 360
8710 ± 80	1.1 ± 0.2	5.7 ± 0.4	690 ± 395
8790–9100	2.4 ± 0.4	5.3 ± 0.4	1775 ± 1025
9130 ± 40	0.4 ± 0.1	6.1 ± 0.4	325 ± 200
$9390 \pm 120^*$	2.2 ± 0.1	5.8 ± 0.3	2130 ± 1265
$9630 \pm 150^*$	1.2 ± 0.3	5.5 ± 0.4	1235 ± 795
$10140 \pm 220^*$	0.8 ± 0.2	5.5 ± 0.4	1315 ± 865
10500 ± 150	0.6 ± 0.1	5.5 ± 0.4	1300 ± 820
10580–11620	0.3 ± 0.1	5.6 ± 0.6	1070 ± 790

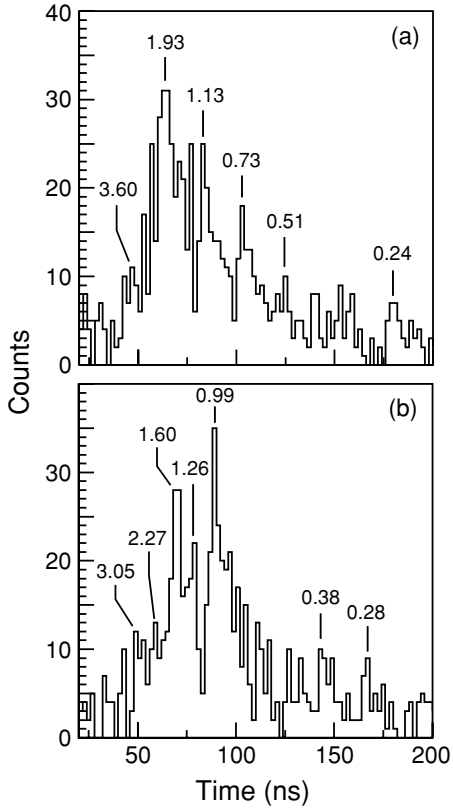

FIG. 15. Time-of-flight spectra measured with the TONNERRE array in coincidence with the (a) 1718 and (b) 2377 keV γ transitions in ^{51}Ca. Neutron energies are in MeV.

In the decay scheme of ^{52}K (Fig. 17), two levels very close in energy are located at 5950 and 5951 keV, respectively. We consider these as separate states because the latter one has been precisely placed above the ground state by a 3388–2563 γ-γ coincidence, whereas the energy of the former relies entirely on the S_{1n} of ^{52}Ca, which is known to only 700 keV. Here

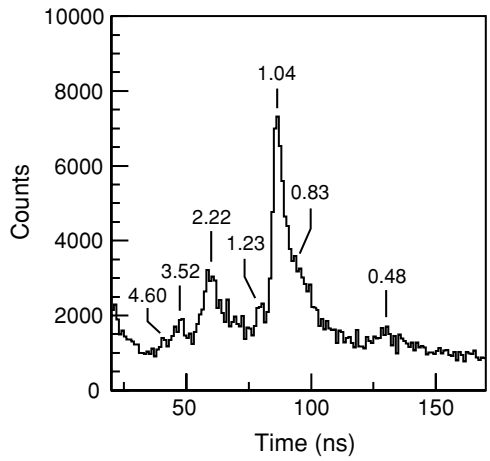

FIG. 16. Time-of-flight spectrum measured with the TONNERRE array corresponding to the feeding of the ^{51}Ca ground state. Neutron energies are in MeV.

we discuss the nature of the 5951 keV level that decays by γ emission.

The preferred radiative deexcitation of the 5951 keV level is not obvious. Levels above the neutron separation energy are expected to be strong neutron emitters with a neutron width Γ_n typically 10^5 times greater than the radiative width Γ_γ. In the framework of the optical model and using an average Woods-Saxon potential, Γ_n is proportional to the neutron penetrability T_ℓ with

$$\Gamma_n = \frac{T_\ell}{2\pi\rho}, \tag{11}$$

where ℓ is the momentum carried by the neutron and ρ is the level density in MeV^{-1}. It has been shown that for $A = 52$, the neutron penetrabilities are much smaller for $\ell = 1$ and 3 than for $\ell = 0$ or 2 [37], T_3 being very small for low-energy neutrons ($E_n \leqslant 2$ MeV). For the radiative deexcitation to be a competitive decay mode of the 5951 keV level, only the emission of a neutron with an angular momentum $\ell = 3$ and $T_3 = 7.3 \times 10^{-4}$ is probable.

In the case of the 5951 keV level, the only accessible state by particle emission is the $3/2^-$ ground state of ^{51}Ca, with a 1.29 MeV neutron transition, if we assume an S_{1n} of 4700 keV. To decay by emission of an $\ell = 3$ neutron, this state must be of positive parity and its spin must be greater than 4 based on momentum conservation laws. The only possibility that meets these conditions and the selection rules of first-forbidden Gamow-Teller transitions is $J^\pi = 4^+$. This assumption is in fair agreement with the observation of a γ transition connecting this state with the 2^+ state at 2563 keV. The possibility of a non-natural parity state is not, however, completly excluded.

We have observed, after delayed neutron emission, five bound states and one unbound state in ^{51}Ca. All these levels, except the one located at 3460 keV, are not populated by direct β decay of ^{51}K (Sec. IV A). The observation of these states through β-γ-n coincidence measurements indicates that they must be of negative parity and fed by $\ell = 0$ or $\ell = 2$ neutron emission from nonnatural parity states in ^{52}Ca. The determination of the spin of these excited states in ^{51}Ca is not straightforward. The Gamow-Teller selection rules for transitions from a possible 2^- ^{52}K ground state and the momentum conservation laws are consistent with a large number of spins ($1/2 \leqslant J \leqslant 11/2$). However, the observation of γ transitions directly feeding the $3/2^-$ ground state of ^{51}Ca suggests that the 1718, 2377, 2934, 3460, and 3500 keV states have spins $J \leqslant 7/2$ as $E2$ transitions are the most favored in that case.

VI. DECAY OF ^{53}K

A. Results

Figure 18(a) presents the β-delayed γ-ray spectrum registered during the β decay of ^{53}K and shows the transitions observed in the first 500 ms of each measurement cycle after subtraction of the background and long-lived daughter activities. Only three transitions are observed at 2220, 2563,

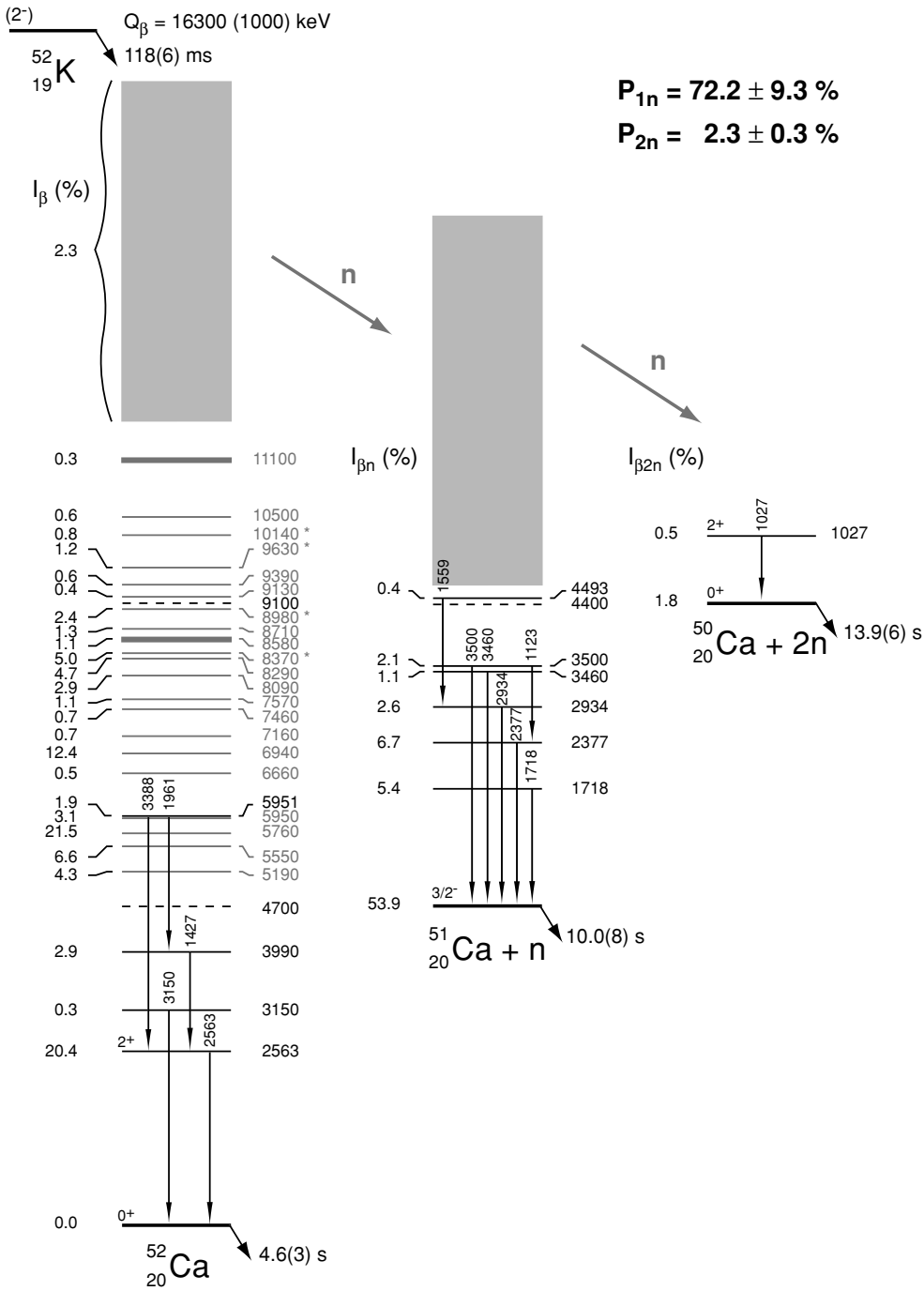

FIG. 17. Same as Fig. 8, but for ^{52}K.

and 3150 keV. The latter two were already observed in the decay of ^{52}K and have been assigned to the level scheme of ^{52}Ca (Sec. V A). The assignment of the remaining 2220 keV γ line is not straightforward. However, since it is not seen in coincidence with delayed neutrons [Fig. 18(b)], it is most likely part of the ^{53}Ca or ^{53}Sc level schemes. To further investigate this transition, we studied the time evolution of its intensity in intervals of 100 ms and found that the behavior of the 2220 and 2563 keV transitions were comparable; based on this, we assigned the 2220 keV γ line to the level scheme of ^{53}Ca. The energies and absolute γ intensities of all transitions are listed in Table IX. The absolute γ intensities were determined using Eq. (8) and the absolute ^{53}K activity.

TABLE IX. Energies and absolute intensities of γ transitions in ^{53}Ca and ^{52}Ca following the β decay of ^{53}K.

Nucleus	E_γ (keV)	I_γ^{abs} (%)	E_i (keV)	E_f (keV)
^{53}Ca	2220 ± 1	15.3 ± 3.3	2220	0
^{52}Ca	2563 ± 1	51.5 ± 9.1	2563	0
^{52}Ca	3150 ± 2	12.4 ± 2.9	3150	0

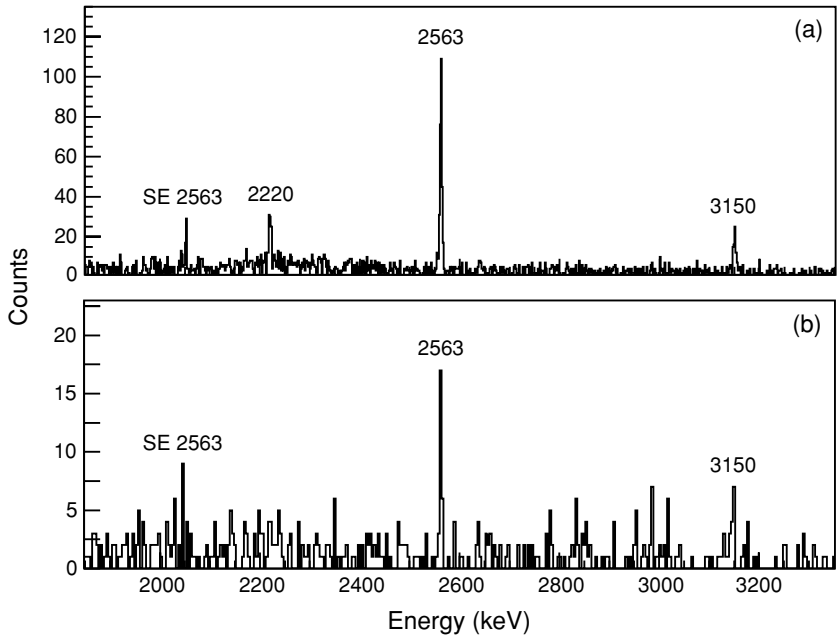

FIG. 18. ^{53}K decay: (a) γ-ray spectrum of activity recorded in the first 500 ms of each measurement cycle. Data are corrected for background and long-lived daughter activities. (b) γ-ray spectrum in coincidence with neutrons detected by the TONNERRE array. Labels are the same as in Fig. 5.

From the absolute intensity of the 2220 keV γ line in ^{53}Ca, one can estimate an upper limit to the contribution of the $1n$- and $2n$-delayed emissions to the total decay strength. The calculation yields $P_{1n} + P_{2n} = 85 \pm 19\%$ assuming no feeding of the ^{53}Ca ground state. In addition, the intensities of the 2563 and 3150 keV transitions provide a lower limit of $64 \pm 11\%$ for the $1n$-emission probability. Limits on the P_{2n} are more difficult to obtain since the most intense transition in the decay of ^{51}Ca, namely, the 861 keV line, is only just visible in the direct γ spectrum. Based on the intensity of the 861 keV transition, we estimate an upper limit of $P_{2n} = 10 \pm 5\%$. The direct production of ^{53}Ca and the possible $1n$ channel feeding of excited states in ^{52}Sc prevent any precise estimate of the P_{1n} value for ^{53}Ca from the analysis of the γ transitions in ^{52}Sc.

The time-of-flight spectrum of the delayed neutrons measured with the TONNERRE array is shown in Fig. 19. Several peaks are present with neutron energies between 400 and 3500 keV. However it is difficult to assign these transitions to the decay of ^{53}K as the daughter nucleus ^{53}Ca is also a neutron emitter with a similar half-life and a relatively high neutron emission probability (P_n $40 \pm 10\%$ [24]). Moreover, because the statistics for the decay of ^{53}K is very limited, we could not perform a β-γ-n triple coincidence analysis of the data in order to locate unbound states in ^{53}Ca. In Table X, the energies and relative intensities of the neutron transitions following the decay of ^{53}K or ^{53}Ca observed in this experiment are listed. Each neutron transition intensity was corrected from the detection efficiency and was then normalized to the intensity of the most intense transition.

The ^{53}K decay scheme established on the basis of the present work is displayed in Fig. 20. The dashed lines represent the neutron emission thresholds in ^{53}Ca and ^{52}Ca [19]. Because of the limited statistics, it was not possible to place the neutron-emitting states in ^{53}Ca.

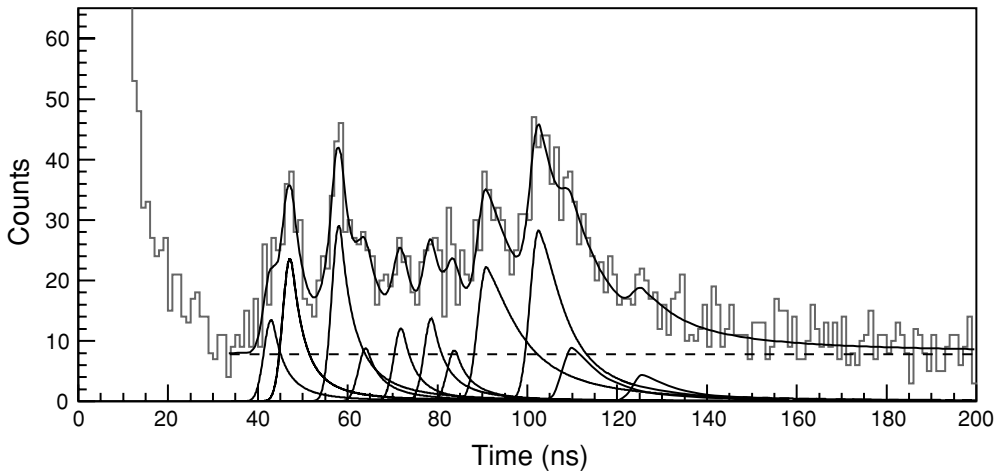

FIG. 19. Same as Fig. 7, but for ^{53}K. Solid lines represent fits to the 11 most significant neutron-transitions.

TABLE X. Energies and relative intensities of delayed neutron transitions following the β decays of ^{53}K and ^{53}Ca.

E_n (keV)	$I_n^{\rm rel}$ (%)
490 ± 10	19 ± 7
640 ± 15	34 ± 11
740 ± 15	100
940 ± 20	99 ± 34
1110 ± 30	19 ± 14
1260 ± 35	32 ± 10
1500 ± 45	26 ± 9
1900 ± 60	23 ± 9
2310 ± 80	87 ± 26
3500 ± 150	64 ± 20
4220 ± 200	39 ± 16

B. Discussion

The spin and parity of the ^{53}K ground state have not been experimentally determined. However, the results obtained for ^{51}K and ^{52}K (Secs. IV A and V A) support the $(d_{3/2})^{-1}$ one-proton hole configuration as being the main component of the ground state wave functions. As the effect of the $p_{1/2}$ neutrons on the relative position of the proton orbitals is not yet understood, we assume that the ground state of ^{53}K is $J^\pi = 1/2^+$ or $3/2^+$. In that case, first-forbidden transitions can feed levels with spins ranging from 1/2 to 7/2. Because of the large $p_{1/2}$-$f_{5/2}$ neutron energy gap (cf. ^{49}Ca level scheme), one expects the ^{53}K ground state to have a dominant $(p_{1/2})^2$ neutron configuration. Hence, the transformations of a $p_{1/2}$ or $p_{3/2}$ neutron are the most probable, and the ^{53}K decay will mainly feed $1/2^-$ and $3/2^-$ states. Figure 21 illustrates these possible Gamow-Teller transitions in the case of a ^{53}K ground state with $J^\pi = 3/2^+$.

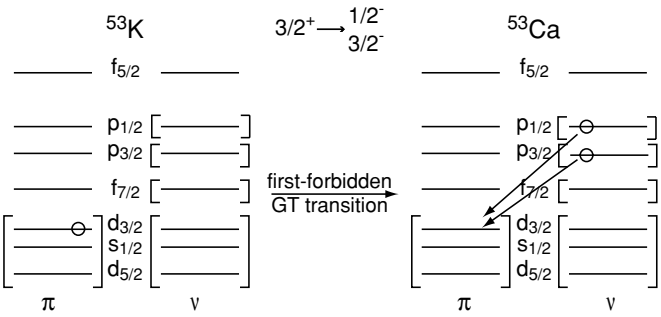

FIG. 21. Left: configuration of the $3/2^+$ ground state in ^{53}K. Right: configurations of the $1/2^-$ and $3/2^-$ excited states in ^{53}Ca, which correspond to the most likely first-forbidden GT transitions with the transformation of a $\nu p_{1/2}$ or $\nu p_{3/2}$ neutron into a $\pi d_{3/2}$ proton.

There is no measurement of the spin and parity of the ^{53}Ca ground state; however, using simple shell-model

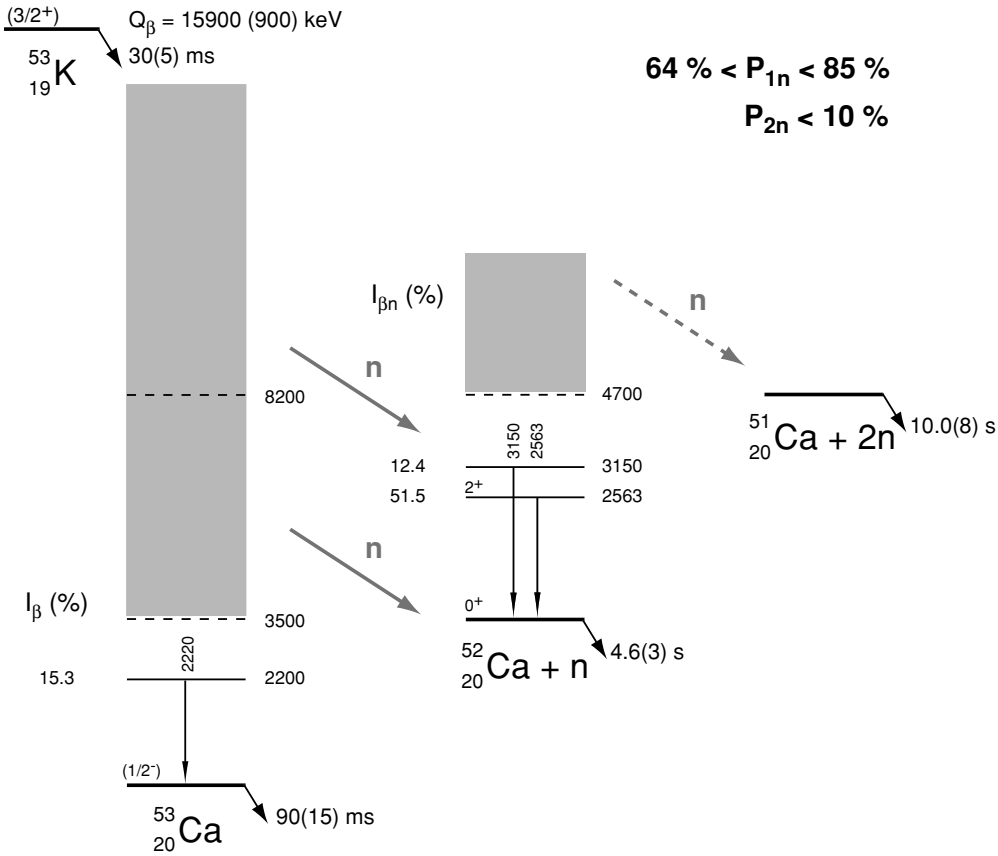

FIG. 20. Same as Fig. 8, but for ^{53}K.

considerations, $J^\pi = 1/2^-$ is expected, corresponding to the configuration where the lone valence neutron occupies the $\nu p_{1/2}$ orbital. The excited state observed at 2.20 MeV is also probably of negative parity, nonnatural parity states being expected at higher energies ($E_x > 3$ MeV). This state might then be the $3/2^-$ state fed by a first-forbidden transition. In that case, it would correspond to a $\nu p_{3/2} \rightarrow \nu p_{1/2}$ neutron excitation.

VII. CONCLUSIONS

We studied the β decays of the neutron-rich potassium isotopes $^{51-53}$K using β-delayed γ, n, and γ-n measurements. Detailed decay schemes to bound and unbound levels in neutron-rich Ca isotopes have been deduced.

Seven γ transitions have been attributed to the β decay of ^{51}K. A total of 25 neutron transition feeding states in ^{50}Ca were observed with a total one-neutron emission probability $P_{1n} = 63 \pm 8\%$. A new level at 3530 keV was identified in ^{50}Ca, and preliminary spin and parity assignments have been made for the ground states of ^{51}K and ^{51}Ca as well as for the excited state at 3.46 MeV in ^{51}Ca.

We observed five new γ transitions in ^{52}Ca following the β decay of ^{52}K and identified three new states at 3150, 3990, and 5951 keV. A total of 25 neutron transition feeding states in ^{51}Ca were observed with a total $1n$ emission probability $P_{1n} = 72.2 \pm 9.3\%$. Eight γ transitions observed in ^{51}Ca in coincidence with neutrons allowed us to place six levels with energies between 1718 and 4493 keV in ^{52}Ca. The $2n$ delayed emission ($P_{2n} = 2.3 \pm 0.3\%$) was observed for the first time.

We also observed for the first time neutron transitions following the β decay of ^{53}K and ^{53}Ca. However, the limited statistics did not allow us to assign these transitions to unbound states in ^{53}Ca or ^{53}Sc. Analysis of the γ-ray and neutron transitions allowed us to fix limits on the P_{1n} and P_{2n} for ^{53}K. Finally, a new state has been identified in ^{53}Ca at 2220 keV. Clearly, a new higher statistics measurement dedicated to the β decay of ^{53}K would be welcome.

The results obtained here should help clarify the structure of neutron-rich fp-shell nuclei around the $N = 32$–34 subshell closures. For a more quantitative understanding, shell-model calculations in the full (fp) valence space using a modified KB3G interaction are currently being carried out. Our experimental data will be compared with the results of these calculations in a forthcoming paper.

ACKNOWLEDGMENTS

We would like to thank our colleagues, engineers, and technicians from IReS-Strasbourg and LPC-Caen, whose collaboration has been so valuable before and during the experiment. We are especially grateful to J.-C. Caspar, D. Etasse, and G. Heitz for their support. We also thank F. Nowacki and E. Caurier for numerous fruitful discussions.

[1] M. G. Mayer, Phys. Rev. **75**, 1969 (1949).
[2] O. Haxel, J. H. D. Jensen, and H. E. Suess, Phys. Rev. **75**, 1776 (1949).
[3] T. Otsuka, R. Fujimoto, Y. Utsuno, B. A. Brown, M. Honma, and T. Mizusaki, Phys. Rev. Lett. **87**, 082502 (2001).
[4] J. I. Prisciandaro, P. F. Mantica, B. A. Brown, D. W. Anthony, M. W. Cooper, A. Garcia, D. E. Groh, A. Komives, W. Kumarasiri, P. A. Lofy, A. M. Oros-Peusquens, S. L. Tabor, and M. Wiedeking, Phys. Lett. **B510**, 17 (2001).
[5] D. E. Appelbe, C. J. Barton, M. H. Muikku, J. Simpson, D. D. Warner, C. W. Beausang, M. A. Caprio, J. R. Cooper, J. R. Novak, N. V. Zamfir, R. A. E. Austin, J. A. Cameron, C. Malcolmson, J. C. Waddington, and F. R. Xu, Phys. Rev. C **67**, 034309 (2003).
[6] P. F. Mantica, A. C. Morton, B. A. Brown, A. D. Davies, T. Glasmacher, D. E. Groh, S. N. Liddick, D. J. Morrissey, W. F. Mueller, H. Schatz, A. Stolz, S. L. Tabor, M. Honma, M. Horoi, and T. Otsuka, Phys. Rev. C **67**, 014311 (2003).
[7] R. V. F. Janssens, B. Fornal, P. F. Mantica, B. A. Brown, R. Broda, P. Bhattacharyya, M. P. Carpenter, M. Cinausero, P. J. Daly, A. D. Davies, T. Glasmacher, Z. W. Grabowski, D. E. Groh, M. Honma, F. G. Kondev, W. Królas, T. Lauritsen, S. N. Liddick, S. Lunardi, N. Marginean, T. Mizusaki, D. J. Morrissey, A. C. Morton, W. F. Mueller, T. Otsuka, T. Pawlat, D. Seweryniak, H. Schatz, A. Stolz, S. L. Tabor, C. A. Ur, G. Viesti, I. Wiedenhöver, and J. Wrzesiński, Phys. Lett. **B546**, 55 (2002).
[8] A. Huck, G. Klotz, A. Knipper, C. Miehé, C. Richard-Serre, G. Walter, A. Poves, H. L. Ravn, and G. Marguier, Phys. Rev. C **31**, 2226 (1985).
[9] T. W. Burrows, Nucl. Data Sheets **76**, 191 (1995).
[10] M. R. Bhat, Nucl. Data Sheets **85**, 415 (1998).
[11] S. N. Liddick, P. F. Mantica, R. V. F. Janssens, R. Broda, B. A. Brown, M. P. Carpenter, B. Fornal, M. Honma, T. Mizusaki, A. C. Morton, W. F. Mueller, T. Otsuka, J. Pavan, A. Stolz, S. L. Tabor, B. E. Tomlin, and M. Wiedeking, Phys. Rev. Lett. **92**, 072502 (2004).
[12] E. Kugler, Hyperfine Interact. **129**, 23 (2000).
[13] J. Eberth, G. Pascovici, H. G. Thomas, N. Warr, D. Weisshaar, D. Habs, P. Reiter, P. Thirolf, D. Schwalm, C. Gund, H. Scheit, M. Lauer, P. Van Duppen, S. Franchoo, M. Huyse, R. M. Lieder, W. Gast, J. Gerl, K. P. Lieb (MINIBALL Collaboration), Prog. Part. Nucl. Phys. **46**, 389 (2001).
[14] M. Bounajma, Ph.D. thesis, Université de Strasbourg 1996, Report No. CRN-96-43 (unpublished).
[15] A. Buţă, T. Martin, C. Timiş, N. Achouri, J. C. Angélique, C. Borcea, I. Cruceru, A. Genoux-Lubain, S. Grévy, M. Lewitowicz, E. Liénard, F. M. Marqués, F. Negoiţă, F. de Oliveira, N. A. Orr, J. Péter, and M. Sandu, Nucl. Instrum. Methods Phys. Res. A **455**, 412 (2000).
[16] J. Rachidi, Ph.D. thesis, Université de Strasbourg 1983, Report No. CRN/PN-83-20 (unpublished).
[17] R. B. Firestone, *Table of Isotopes*, edited by V. S. Shirley (Wiley, New York, 1996), 8th ed., Vol 1, p. 205.
[18] J. Lettry, R. Catherall, P. Drumm, P. Van Duppen, A. H. M. Evensen, G. J. Focker, A. Jokinen, O. C. Jonsson, E. Kugler, H. Ravn (ISOLDE Collaboration), Nucl. Instrum. Methods Phys. Res. B **126**, 130 (1997).
[19] G. Audi, A. H. Wapstra, and C. Thibault, Nucl. Phys. **A729**, 129 (2003).

[20] S. Piétri, Ph.D. thesis, Université de Caen 2003, Report No. LPCCT-02-03 (unpublished). http://tel.ccsd.cnrs/docs/00/04/56/04/PDF/tel-00003438.pdf

[21] L. C. Carraz, P. G. Hansen, A. Huck, B. Jonson, G. Klotz, A. Knipper, K. L. Kratz, C. Miehé, S. Mattsson, G. Nyman, H. Ohm, A. M. Poskanzer, A. Poves, H. L. Ravn, C. Richard-Serre, A. Schroder, G. Walter, and W. Ziegert, Phys. Lett. **B109**, 419 (1982).

[22] S. Grévy, N. L. Achouri, J. C. Angélique, C. Borcea, A. Buţă, F. De Oliveira, M. Lewitowicz, E. Liénard, T. Martin, F. Negoiţă, N. A. Orr, J. Peter, S. Pietri, and C. Timis, Phys. Rev. C **63**, 037302 (2001).

[23] GEANT4 Collaboration, CERN/LHCC 98-44 (unpublished).

[24] M. Langevin, C. Detraz, D. Guillemaud-Mueller, A. C. Mueller, C. Thibault, F. Touchard, G. Klotz, C. Miehé, G. Walter, M. Epherre, and C. Richard-Serre, Phys. Lett. **B130**, 251 (1983).

[25] I. S. Towner, E. Hagberg, J. C. Hardy, V. T. Koslowsky, and G. Savard, in *ENAM95: Exotic Nuclei and Atomic Masses*, Arles, France 1995, edited by M. de Saint Simon and O. Sorlin (Editions Frontières, Gif-sur-Yvette, France, 1995), p. 711.

[26] K. Schreckenbach, P. Liaud, R. Kossakowski, H. Nastoll, A. Bussiere, and J. P. Guillaud, Phys. Lett. **B349**, 427 (1995).

[27] J. Retamosa, E. Caurier, F. Nowacki, and A. Poves, Phys. Rev. C **55**, 1266 (1997).

[28] J. H. Bjerregaard, O. Hansen, O. Nathan, R. Stock, R. Chapman, and S. Hinds, Phys. Lett. **B24**, 568 (1967).

[29] E. Newmann and J. C. Hiebert, Nucl. Phys. **A110**, 366 (1968).

[30] S. Nummela, P. Baumann, E. Caurier, P. Dessagne, A. Jokinen, A. Knipper, G. Le Scornet, C. Miehé, F. Nowacki, M. Oinonen, Z. Radivojevic, M. Ramdhane, G. Walter, J. Aystö (ISOLDE Collaboration), Phys. Rev. C **63**, 044316 (2001).

[31] E. K. Warburton, Phys. Rev. C **44**, 1024 (1991).

[32] P. Baumann, M. Bounajma, F. Didierjean, A. Huck, A. Knipper, M. Ramdhane, G. Walter, G. Marguier, C. Richard-Serre, and B. A. Brown, Phys. Rev. C **58**, 1970 (1998).

[33] C. Détraz, D. Guillemaud, G. Huber, R. Klapisch, M. Langevin, F. Naulin, C. Thibault, L. C. Carraz, and F. Touchard, Nucl. Phys. **A302**, 41 (1978).

[34] R. Abegg, J. D. Hutton, and M. E. Williams-Norton, Nucl. Phys. **A303**, 121 (1978).

[35] E. Kashy, A. Sperduto, H. A. Enge, and W. W. Buechner, Phys. Rev. **135**, B865 (1964).

[36] B. Singh, J. L. Rodriguez, S. S. M. Wong, and J. K. Tuli, Nucl. Data Sheets **84**, 487 (1998).

[37] G. S. Mani, M. A. Melkanoff, and I. Iori, CEA Internal Report No. 2380, 1963 (unpublished).